



Modulation of Diurnal SST and Diurnal Warm Layer Variability by Salinity-Driven Stratification in the Bay of Bengal

Siddhant Kerhalkar,^{a,b} Amit Tandon,^a J.Thomas Farrar,^c Jennifer A MacKinnon,^d Tamara L Schlosser,^e Leah Johnson,^f Andrew J Lucas,^{d,g} Verena Hormann,^d Luca R Centurioni,^d

^a*School for Marine Science and Technology, University of Massachusetts Dartmouth, New Bedford, MA, USA*

^b*School of Ocean and Earth Science and Technology, University of Hawai'i at Manoa, Honolulu, HI, USA*

^c*Department of Physical Oceanography, Woods Hole Oceanographic Institution, Woods Hole, MA, USA*

^d*Scripps Institution of Oceanography, University of California, San Diego, La Jolla, CA, USA*

^e*Institute for Marine and Antarctic Sciences, University of Tasmania, Hobart, Australia*

^f*Applied Physics Laboratory, University of Washington, Seattle, WA, USA*

^g*Department of Mechanical and Aerospace Engineering, University of California, San Diego, La Jolla, CA, USA*

Corresponding author: Siddhant Kerhalkar, siddhant@hawaii.edu

Early Online Release: This preliminary version has been accepted for publication in *Journal of Physical Oceanography*, may be fully cited, and has been assigned DOI 10.1175/JPO-D-25-0134.1. The final typeset copyedited article will replace the EOR at the above DOI when it is published.

© 2025 American Meteorological Society. This is an Author Accepted Manuscript distributed under the terms of the default AMS reuse license. For information regarding reuse and general copyright information, consult the AMS Copyright Policy (www.ametsoc.org/PUBSReuseLicenses).

ABSTRACT: Diurnal cycles of Sea Surface Temperature (SST) are important for ocean–atmosphere coupling. However, observations of their lateral variability, especially in freshwater-dominated regions and in presence of Diurnal Warm Layers (DWLs), remain limited. This study investigates the spatial differences in the diurnal SST amplitude (during DWL and non-DWL days) and subsurface DWL evolution in the Bay of Bengal using remote sensing, in-situ observations, and 1-D modeling. While satellite data reveal $O(1\text{ }^{\circ}\text{C})$ differences in diurnal SST amplitude over 100 km, in-situ observations uncover finer-scale and more extreme variability, especially during DWL events. We observe that differences in diurnal SST amplitude over mesoscale and smaller lengths ($< 100\text{ km}$) are larger during DWL days (median: $0.2\text{ }^{\circ}\text{C}$, extreme: $1.4\text{ }^{\circ}\text{C}$) when compared to non-DWL days (median: $0.1\text{ }^{\circ}\text{C}$, extreme: $0.2\text{ }^{\circ}\text{C}$). Observations from drifters and complementary 1-D model simulations reveal that lateral differences in salinity-driven stratification leads to diurnal SST amplitude differences of about 0.2°C for shallow mixed layer scenarios ($< 8\text{ m}$). While stratification differences explain the median variability in diurnal SST amplitude, extreme differences in diurnal SST require additional contributions from spatial variations in surface forcing and optical properties. Observations also reveal that lateral differences in salinity stratification modify the DWL response, leading to $O(10\text{ m})$ differences in DWL depth, making it the same order as typical MLD scales in the Bay. These results highlight the critical role of small-scale differences in salinity-driven stratification (set by rainfall and mesoscale flow fields in the Bay) in causing diurnal SST and DWL response differences.

SIGNIFICANCE STATEMENT: The daily cycle of Sea Surface Temperature (SST) plays a key role in ocean–atmosphere heat and moisture exchange. This effect is particularly enhanced during the presence of Diurnal Warm Layers, which are anomalously warm upper-ocean layers formed during low wind speeds. This study explores how daily SST warming varies over distances less than 100 km. Using satellite and in-situ data from the Bay of Bengal, we find that warming can differ by up to 1 °C across around 100 km. These differences arise partly from salinity-driven stratification, but variations in surface forcing and water optics also play a role. Understanding these patterns is important because they affect the ocean and atmosphere interaction, influencing atmospheric convection and weather.

1. Introduction

The diurnal cycle of sea surface temperature (SST) is primarily driven by daily variations in incoming shortwave radiation (SWR, Kondo et al. 1979; Imberger 1985; Price et al. 1986; Lotlike et al. 2016). Part of the incoming SWR warms the top few meters and leads to the formation of a stratified diurnal warm layer (DWL) in the presence of light-to-moderate wind speeds (Imberger 1985; Fairall et al. 1996b; Stuart-Menteth et al. 2005; Soloviev and Lukas 2006). DWLs typically have vertical scales of $O(10\text{ m})$ and spatial scales of up to $O(1000\text{ km})$ (Soloviev and Lukas 1997; Prytherch et al. 2013; Bellenger and Duvel 2009). The stratification within the DWL traps momentum and heat within it, causing temperature anomalies of $O(0.1\text{-}1\text{ }^{\circ}\text{C})$ and near-surface velocity anomalies of $0.1\text{-}0.3\text{ m s}^{-1}$ as compared to the bulk of the mixed layer (Price et al. 1986; Sutherland et al. 2016; Shcherbina et al. 2019; Hughes et al. 2021). The momentum trapping within the DWL leads to high vertical shear, which is destabilizing in nature and competes with the stabilizing heat-driven stratification (Price et al. 1986; Sutherland et al. 2016; Hughes et al. 2020a, 2021). This shear starts dominating in the afternoon once the incoming SWR reduces, causing the DWL to deepen (e.g., Hughes et al. 2021). The DWL is mixed away during the night-time convective mixing (e.g., Hughes et al. 2020a).

DWLs impact air-sea interaction over various time-scales. In the equatorial Indian Ocean, the presence of DWLs induces a deviation in the diurnal cycle of atmospheric convection. This deviation is evident through a secondary peak in convection during the afternoon, which occurs alongside the typical primary maximum in the convection in the early morning (Bellenger et al. 2010;

de Szoek et al. 2021). The inclusion of DWLs in bulk flux calculations results in an instantaneous difference of up to 50 W m^{-2} in the air-sea fluxes compared to non-DWL-resolving calculations (Clayson and Bogdanoff 2013). The inclusion of the DWL effects in coupled atmosphere-ocean models improves the representation of deep convection and enhances the predictability of the seasonal phenomena like the Madden-Julian Oscillation (MJO) and monsoons (Seo et al. 2014; Pradhan et al. 2022; Song et al. 2024).

Traditionally, DWLs have been conceptualized as one-dimensional features dependent on SWR, wind speeds and the optical properties of water (Price et al. 1986; Webster et al. 1996; Stuart-Menteth et al. 2005; Merchant et al. 2008; Thompson et al. 2019). However in regions like the Bay of Bengal, freshwater fluxes from rainfall and rivers significantly modify the background stratification. Mesoscale eddies redistribute this freshwater throughout the Bay, influencing both the vertical stratification and creating salinity fronts over $O(10 \text{ km})$, referred to as mesoscale-structured stratification (Sengupta and Ravichandran 2001; Shenoi et al. 2002; Rao and Sivakumar 2003; Sengupta et al. 2006; Mahadevan et al. 2016; Sengupta et al. 2016; Wijesekera et al. 2016; Sree Lekha et al. 2018, 2020). Anecdotal observations suggest that such mesoscale-structured stratification may influence diurnal cycles of SST and DWL evolution, trapping heat to a shallower depth (e.g., Shroyer et al. 2016). Since DWLs respond to surface forcing and background stratification, lateral variability in these factors over mesoscale and smaller length scales (observed in other ocean basins, e.g. Nuijens et al. 2024; Song et al. 2022; Sengupta et al. 2016) may lead to spatial differences in DWL evolution and influence atmospheric boundary layer dynamics through air-sea coupling.

Despite multiple satellite-based studies detecting lateral gradients in diurnal SST amplitudes (Merchant et al. 2008; Gentemann et al. 2008; Marullo et al. 2016), the influence of lateral variability in background stratification on diurnal SST amplitude and DWLs remains largely unexplored at mesoscale and smaller lengths. Investigating these gradients using satellite observations is challenging due to cloud cover, satellite pass times, and the lack of vertical structure information. Furthermore, microwave remote sensing products (including salinity) currently cannot resolve features at length scales finer than about 50 km (though gridded at 25 km, Wentz et al. 2014; Entekhabi et al. 2014).

The primary objective of this study is to assess how salinity-driven stratification modulates lateral differences in diurnal SST amplitudes and the subsurface structure of DWLs across mesoscale and smaller scales in the Bay of Bengal. In addition, we quantify the overall magnitude of lateral differences in diurnal SST during DWL events, which are influenced by variability in surface forcing and stratification over $O(10$ km). We pose the following questions:

- How do variations in salinity-driven stratification modulate lateral differences in diurnal cycles of SST and the subsurface evolution of DWLs?
- Given that surface forcing also varies over $O(100$ km), how do in-situ differences in diurnal SST respond across $O(1-100$ km) during DWL events?

To address these questions, we use in-situ observations from the ASIRI (Air–Sea Interactions in the Northern Indian Ocean, Wijesekera et al. 2016) and MISO-BoB (Monsoon Intra-seasonal Oscillations in the Bay of Bengal, Shroyer et al. 2021) field campaigns conducted in 2015 and 2019 respectively. We also employ a one-dimensional turbulence model to examine the effects of salinity stratification on variability in diurnal SST amplitudes and DWL evolution. In section-2, we describe the remote sensing and observational datasets, methods and models used in this study. Next, we describe the comparison of lateral variability in diurnal SST amplitudes from remote sensing and surface drifters as well as mooring triad network (Section 3). Then we describe the in-situ differences in diurnal cycles and investigate the role of salinity stratification (Section 4,5). We additionally show an example of how differences in salinity stratification over $O(30$ km) length creates differences in the vertical evolution of Diurnal Warm Layers (Section 6). The broader implications of this research are discussed in Section 7, with a summary of findings in Section 8.

2. Data and Methods

a. Data Sources

1) ASIRI FIELD CAMPAIGN IN 2015

Forty-six surface drifters (Niiler et al. (1995), see <https://gdp.ucsd.edu/ldl/svps/> for their technical details) drogued at 15 m depth were deployed in the Northern Bay as a part of ASIRI (Wijesekera et al. 2016; Hormann et al. 2016). Deployed in ten groups of four to five drifters each, they were released along the periphery of a mesoscale cyclonic eddy and in proximity to a

pronounced salinity front (see Figure-1 a,b in Essink et al. 2019). This arrangement resulted in drifter pair separations ranging from 0.5 to 30 km. The drifters measured the surface temperature at 0.2 m depth and salinity at 0.5 m depth (with an accuracy of 0.05 °C and 0.003 g/kg respectively). The drifters sampled every 5 minutes during the field campaign (23 August–21 September 2015), and every 30 minutes thereafter. More details on deployment and the quality control can be found in Hormann et al. (2016) and Essink et al. (2019). This study uses drifter data from September to November 2015, covering the Fall Intermonsoon and Northeast Monsoon seasons (based on season classifications in Weller et al. 2019).

A triad mooring network in the northern Bay of Bengal collected simultaneous atmospheric and oceanographic data during 2015, spanning all the seasons (Weller et al. 2019). This network consisted of two long-term operational sites maintained by the India's National Institute of Ocean Technology (NIOT, BD08 at 18.2°N, 89.7°E and BD09 at 17.9°N, 89.7°E) and a third mooring deployed by the Woods Hole Oceanographic Institution (WHOI) for the ASIRI campaign at 18.0°N, 89.5°E. The three moorings were approximately 30 km apart (see Figure 1b and Figure 2a in Simoes-Sousa et al. 2022). Further details on mooring instrumentation can be found in Weller et al. (2016, 2019) and Simoes-Sousa et al. (2022).

2) MISO-BoB FIELD CAMPAIGN IN 2019

Thirty surface drifters were deployed about 300 km off the Indian coast in the western side of the Bay of Bengal during the MISO-BoB field campaign (06 July to 04 August 2019, which span the Summer Monsoon period, Local time = UTC + 5.5 hours). Initially spaced 20 km apart, these drifters were similar to those used in 2015 but lacked surface salinity sensors (Figure A1). The drifters mostly followed a mesoscale anticyclonic eddy (indicated by letter A in Figure A1) and measured surface temperature and sea level pressure (SLP) every 15 minutes.

Additionally, three Drogued-Buoy Air Sea Interaction Systems (D-BASIS¹; referred to as D1, D2 and D3), were deployed to simultaneously measure the air-sea fluxes and upper-ocean structure (Figure A1). Each D-BASIS profiler consists of a WHOI surface buoy (similar to the 2015 mooring discussed above) equipped with meteorological sensors. Meteorological data were recorded at 1-minute intervals and averaged to 15-minute resolution to match that of the surface drifters. Bulk air-sea fluxes from these measurements are calculated using the COARE 3.6 algorithm (Fairall

¹named in honor of the esteemed Indian oceanographer, Prof. Debasis Sengupta

et al. 1996b, 2003). Due to a damaged radiometer on D3, SWR data from nearby D2 (initially deployed 40 km away and coming as close as 20 km, Figure A1b) was used to calculate the air-sea fluxes for D3.

Each D-BASIS profiler also carries a Scripps Institution of Oceanography (SIO) Wirewalker (Pinkel et al. 2011; Zheng et al. 2022). This wave-powered profiler continuously sampled the upper 100 m of the ocean. The Wirewalker profiler measured subsurface temperature, salinity, velocity, thermal microstructure, bio-optical properties and underwater spectral irradiance at a vertical resolution of 0.25 m. The measurements taken during the smooth upward motion of the profiler are used here. Hence, the effective time resolution between profiles was nearly 10 minutes. The D-BASIS had drag elements attached to the line at 200 m depth as to ensure that it drifted at a typical speed of 0.2-0.3 m s⁻¹ with currents. For the analysis using drifters and D-BASIS profilers from this field campaign, we restrict the data to the period between 07 and 28 July 2019.

Spatial variability in the central Bay was assessed using a rapid profiling shipboard system FastCTD (e.g., MacKinnon et al. 2021). It profiles the temperature and salinity in the upper 200 m while the ship moves at 2-5 knots. The vertical resolution of the FastCTD dataset was 1 m and each profile took 1.5 minutes to complete, giving a typical horizontal resolution of 210 m.

b. Remote Sensing

We use daily SST data from the Advanced Microwave Scanning Radiometer 2 (AMSR-2; <https://www.remss.com/missions/amsr/>) aboard the AQUA satellite. This satellite operates in a sun-synchronous orbit with a 1:30 AM/PM equator crossing time. The daily version of AMSR-2 provides SST measurements at an effective resolution of 46 km (despite being gridded on a 25 km scale, Wentz et al. 2014). Daytime and nighttime satellite passes from September to November 2015 and from July to August 2019 are used to infer the diurnal SST amplitude.

In order to distinguish the role of rainfall-induced stratification and mesoscale-structured stratification, we use data from IMERG (Integrated Multi-satellitE Retrievals for Global precipitation measurement, <https://gpm.nasa.gov/data/imerg>, Huffman et al. 2015) for 17 and 18 July 2019. This dataset has a time resolution of 30 minutes and a spatial resolution of 10 km.

c. Models

General Ocean Turbulence Model (GOTM) provides a one-dimensional ocean model framework that includes various vertical mixing schemes (Burchard et al. 1999). GOTM also provides flexibility to choose the stability functions, wave breaking and internal wave parameterizations. GOTM with the $k - \epsilon$ mixing scheme (which involves a subgrid-scale kinetic energy (k) and the subgrid dissipation (ϵ) parameterization) has been used in previous studies to accurately model the diurnal variability in SSTs, thermal stratification, salinity and Turbulent Kinetic Energy (TKE) dissipation rate (Pimentel et al. 2008; Johnson et al. 2023; Burchard and Bolding 2001; Drushka et al. 2016; Burchard et al. 2002; Schmitt et al. 2024). We use the two-equation $k-\epsilon$ turbulence closure scheme with the dynamic dissipation rate length scale along with the Canuto A version of the stability function (Canuto et al. 2001). With the exception of the omitted internal wave breaking parameterization, all other settings align with GOTM's default options (see Burchard et al. 1999). Each GOTM simulation is performed for a 24-hour period and is initialized at sunrise. The vertical and temporal resolution for GOTM runs are 0.05 m and 1 minute respectively. The prescribed surface forcing conditions and optical properties of water vary across cases and are detailed in Sections 5 and 6.

d. Methods

1) QUANTIFYING THE DIURNAL SST AMPLITUDES

Diurnal SST amplitude from remote sensing is estimated as the difference in SSTs between daytime and nighttime passes, which occur at approximately 1:30 pm (close to the typical time of maximum SST in the diurnal cycle) and 1:30 am local time respectively. The drifter measurements are synchronized with the satellite pass times to enable direct comparison between remote sensing and in-situ drifters.

For the in-situ analysis, we quantify the diurnal SST amplitude by using the concept of foundational temperature (T_f , Donlon et al. 2007; Prytherch et al. 2013). T_f is defined as the temperature just before sunrise for each day (6 am to 6 am the next day) and for each drifter/D-BASIS profiler/Mooring. Linear interpolation between the T_f points is performed to describe the SST tendency at time scales longer than diurnal. The diurnal SST amplitude is then calculated as the

peak difference between the SST and the interpolated T_f over midday hours (e.g., 12:00–15:00 local time, when the diurnal cycle typically reaches its maximum).

2) CLASSIFICATION OF DWL-CONDUCIVE DAYS BASED ON OBSERVATIONS

Detecting DWLs typically requires well-resolved vertical profiles of temperature, stratification, and shear (e.g., Thompson et al. 2019), such as those provided by the D-BASIS profilers (see Appendix A). However, such detailed measurements are not available from the triad mooring network or surface drifters due to their coarse vertical resolution. To address this limitation, we follow Thompson et al. (2019) and use a threshold-based classification scheme to identify DWL-condusive (DWL-C) days at the triad moorings. Specifically, DWL-C days are classified as those with mean wind speeds below 6 ms^{-1} (measured at 3 m height) and peak shortwave radiation (SWR) exceeding 750 W m^{-2} . Conversely, other days not meeting these criteria are classified as DWL-NC (not conducive to DWL formation).

These thresholds are based on both our D-BASIS observations (Appendix A) and limits established in prior studies (Thompson et al. 2019), and are consistent with conditions favorable for DWL formation in past work (Prytherch et al. 2013; Hughes et al. 2020a,b, 2021). For drifters, which do not measure wind or surface fluxes directly, we assign DWL-C or DWL-NC classifications based on the periods identified at the Triad moorings and D-BASIS (as long as drifters are within a 1000 km radius of the Triad mooring/D-BASIS). This assumption is supported by the broad spatial extent of DWLs (e.g., Bellenger and Duvel 2009).

3) METRIC FOR DWL DEEPENING DEPTH

We use the depth of the maximum temperature gradient ($z_{T_{z_{max}}}$) to determine the depth of the DWL from the observations in D-BASIS profilers and GOTM simulations (Hughes et al. 2020b). This method is used because the temperature is well-resolved vertically in these datasets, thereby allowing its vertical gradient (T_z) to be treated as a continuous quantity. This parameter cannot be tracked in the 2015 triad mooring network due to its vertically discrete temperature measurements.

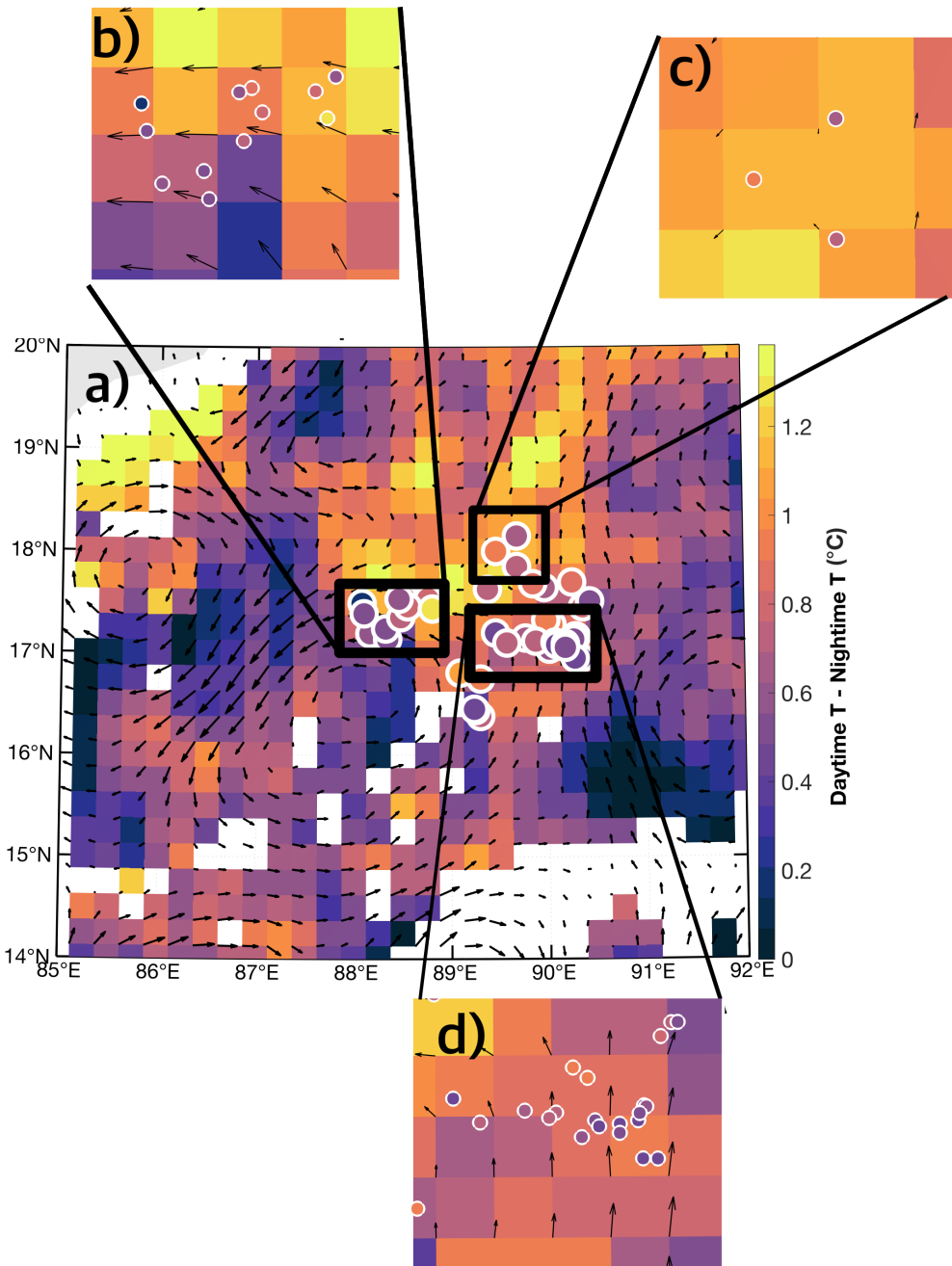


FIG. 1. a) Difference between daytime and nighttime temperatures on 26 September 2015 from AMSR-2, with colored circles denoting the same quantity from in-situ drifters and the triad mooring network. b), c), d) Zoomed views of regions within the boxes in a). Black arrows indicate the geostrophic currents on 26 September 2015, while the white points in a) indicate missing data.

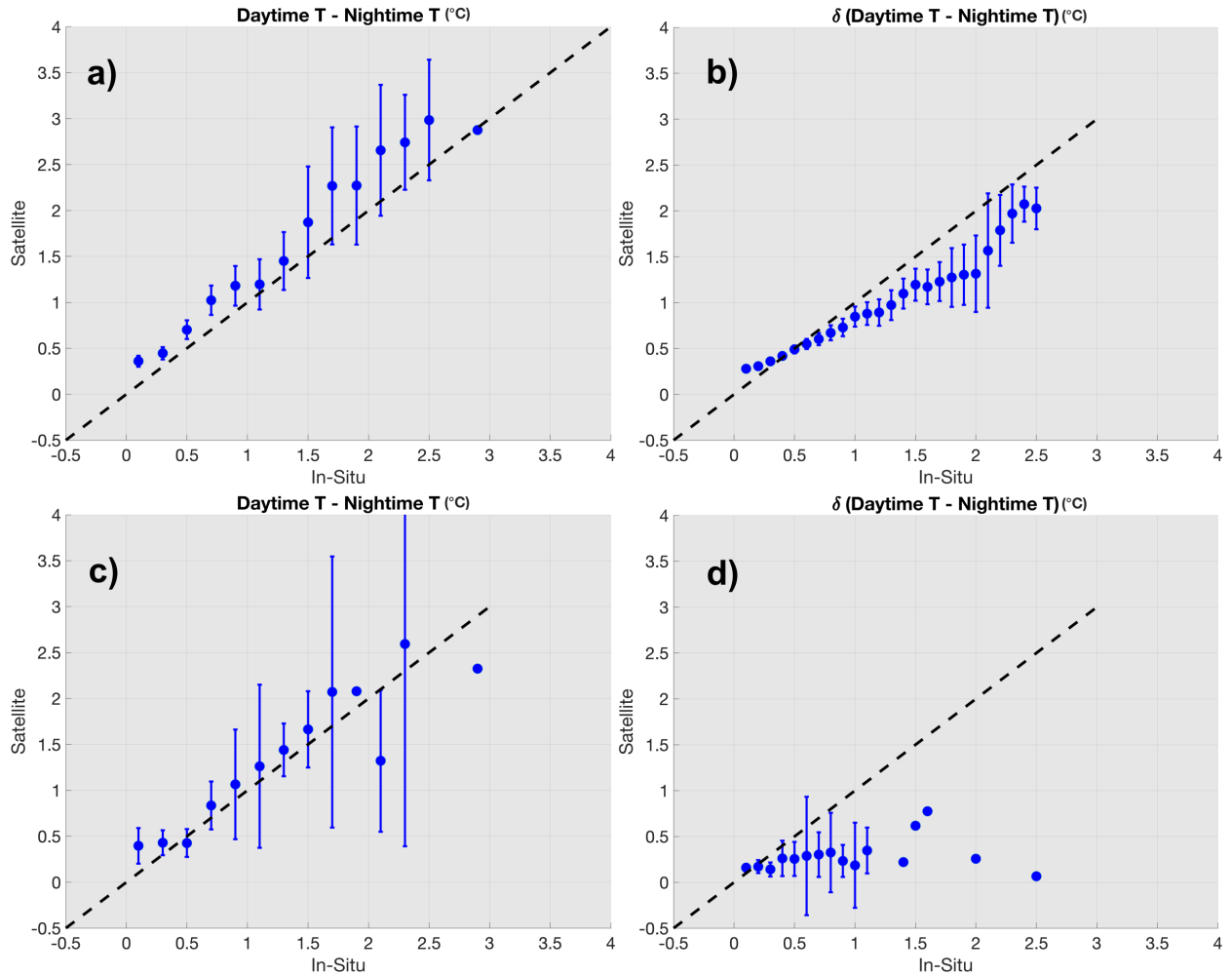


FIG. 2. a) Detailed comparison of binned differences in daytime and nighttime temperature from in-situ drifters and corresponding remote sensing measurements from 01 September to 30 November 2015 and 06 July to 04 August 2019. b) Comparison of lateral contrasts in daytime and nighttime temperature differences from in-situ drifters over length scales of 50 km and more as well as corresponding remote sensing measurements. The dashed lines in a) and b) indicate the line of equality. The error bars indicate three standard deviations of the satellite measurements within the bin. c) and d) are the same as a) and b) except for in-situ triad mooring network between 01 January and 31 December 2015.

3. Comparison of remote sensing and drifters in capturing lateral variability in diurnal SST amplitude

In-situ observations from moorings and drifters are often unavailable over mesoscale length scales ($O(100 \text{ km})$) in the Bay, highlighting the value of remote sensing for capturing lateral

differences in diurnal SST. To assess the accuracy of AMSR-2 in resolving these patterns, we compare the AMSR-2 diurnal SST magnitudes and differences with drifters and the triad mooring network during September–November 2015.

Overlaying in-situ diurnal SST magnitudes ($\Delta T_{diurnal}$) onto AMSR-2 maps for a specific day (26 September 2015) indicates that the large-scale spatial patterns observed in remote sensing are generally consistent with those inferred from drifter observations (Figure 1a). However, a closer examination of in-situ observations within individual AMSR-2 grid boxes (Figure 1a) reveals pronounced contrasts in $\Delta T_{diurnal}$ among drifters, with differences as large as 0.4 °C (Figure 1b,c,d). This indicates significant lateral variability in diurnal SST at scales smaller than the AMSR-2 spatial resolution (50 km or less).

To extend our comparison over three months, we analyzed AMSR-2 $\Delta T_{diurnal}$ and their lateral differences ($\delta(\Delta T_{diurnal})$), contrasting them with in-situ observations from drifters and the triad mooring network. We observe that satellite-derived $\Delta T_{diurnal}$ are consistently higher than in-situ values by approximately 0.2–0.3°C. These discrepancies increase up to 0.5°C for drifter observations on days with strong diurnal warming (greater than 1.5°C, Figure 2a,c). These larger in-situ $\Delta T_{diurnal}$ are also associated with greater uncertainty in the satellite estimates. Potential sources of such discrepancies include the mismatch in the measurement depth (where the drifters measures the bulk temperature while AMSR-2 measures the skin temperature of the ocean) as well as presence of lateral differences in diurnal cycles of SST over mesoscale and smaller length scales.

While AMSR-2 tends to overestimate the overall $\Delta T_{diurnal}$, it underestimates the $\delta(\Delta T_{diurnal})$. Both drifter pairs (separations >50 km) and the triad mooring network (approximately 30 km spacing) show significantly higher $\delta(\Delta T_{diurnal})$ than corresponding AMSR-2 estimates (Figure 2b,d). While moderate lateral differences show a 0.2–0.3 °C satellite underestimation, the bias worsens under strong $\delta(\Delta T_{diurnal})$ values. The mismatch remains evident even at drifter pair separations exceeding the satellite’s resolution, suggesting that satellite products underestimate lateral variability in diurnal SSTs, particularly during strong difference events. The triad mooring comparisons further emphasize considerable mesoscale and submesoscale variability (<50 km) unresolved by satellites. Building on these findings, we next analyze the in-situ $\Delta T_{diurnal}$ from the 2015 and 2019 field campaigns, classifying them into DWL-C and DWL-NC days.

4. In-Situ Observations of $\Delta T_{diurnal}$ and $\delta(\Delta T_{diurnal})$ in presence and absence of DWLs

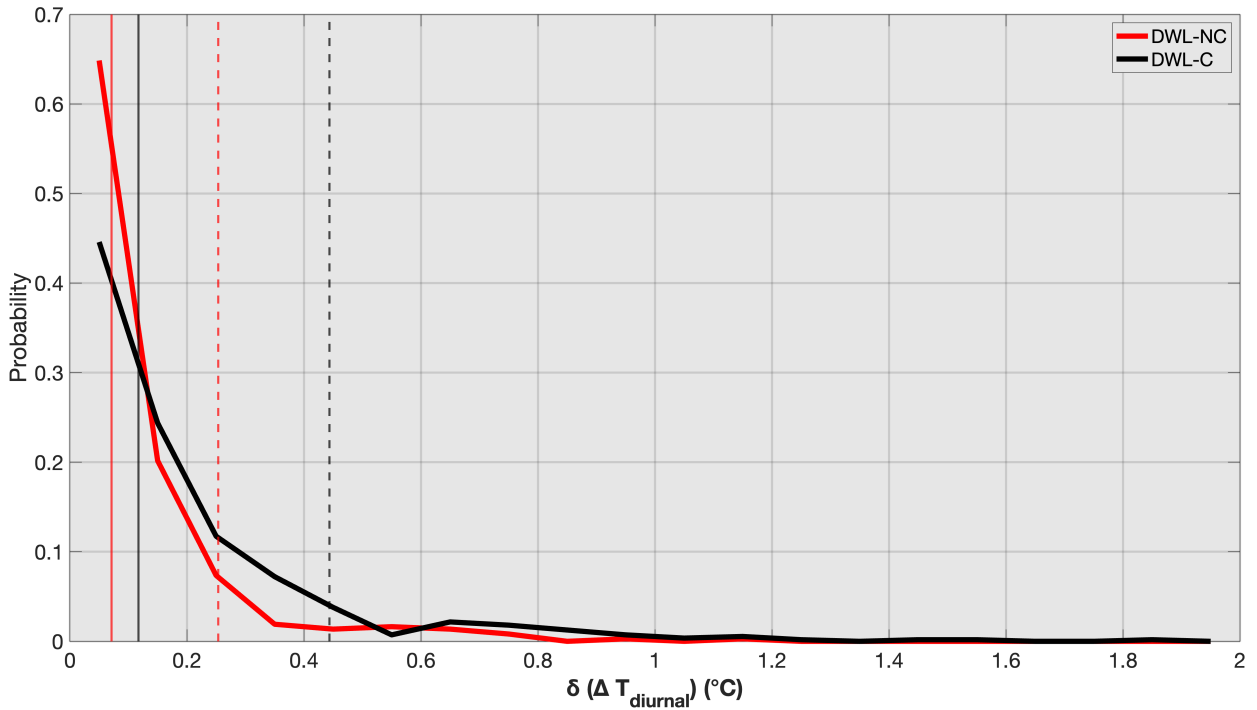


FIG. 3. Probability Distribution Function of spatial differences in Diurnal SST magnitudes ($\delta(\Delta T_{diurnal})$) from the triad mooring network for DWL-NC days (red line) and expected DWL-C days (black line). The corresponding vertical solid lines indicate the median values while the dashed lines indicate the 90th percentile values for the DWL-NC and DWL-C days.

Using the thresholds defined in Section 2 (subsection-d, 2), we identify 188 DWL-C days in the triad mooring network during 2015. While the probability distributions of $\delta(\Delta T_{diurnal})$ for DWL-C and DWL-NC days from the triad mooring network are broadly similar (Figure 3), the $\delta(\Delta T_{diurnal})$ below 0.1°C are less likely to occur on DWL-C days (45%) than on DWL-NC days (65%). The median $\delta(\Delta T_{diurnal})$ is 0.11°C for DWL-C days, compared to 0.07°C for DWL-NC days. Notably, the 90th percentile values for $\delta(\Delta T_{diurnal})$ for DWL-C and DWL-NC days are 0.48°C and 0.28°C respectively. This indicates that spatial inhomogeneity in diurnal SST is more pronounced during DWL-C days. However, this result is derived from a relatively small dataset (approximately 1,000 data points) collected from a mooring network with a fixed spacing of 30 km. While the observations span the entire year, the fixed separation limits the ability to assess variability across a broader range of spatial scales.

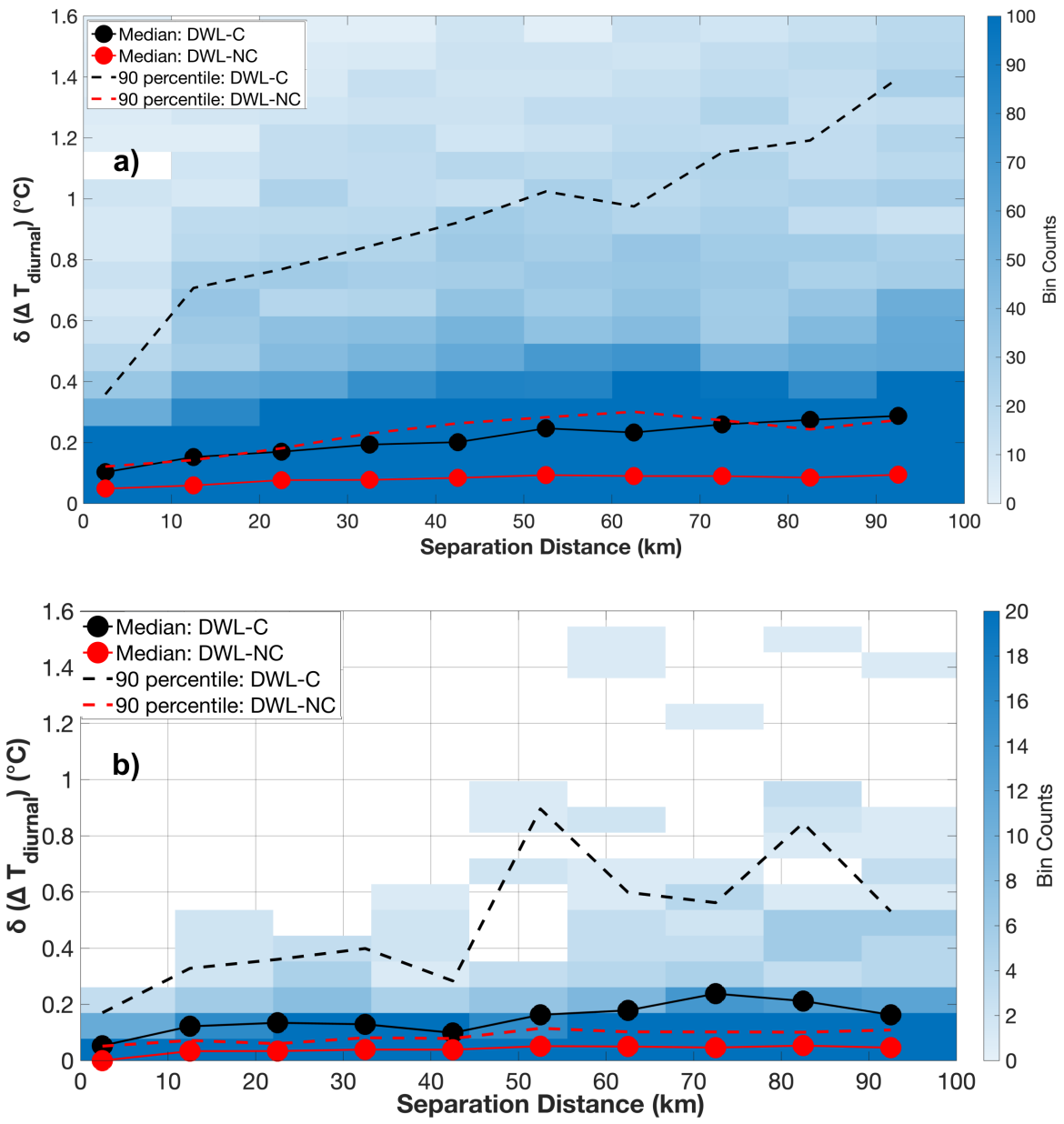


FIG. 4. Binned scatter plot of spatial differences in diurnal SST magnitudes ($\delta(\Delta T_{diurnal})$) between drifter pairs versus their separation distances for (a) 01 September to 30 November 2015 (11,186 observations) and (b) 06 July to 04 August 2019 (1,207 observations). Color indicates the number of observations per bin (every 10 km and 0.1 °C). Solid lines with circle markers show the median values in each separation-distance bin, separated into DWL-C days (black) and DWL-NC days (red). Dashed lines indicate the 90th percentile values in each bin.

We conduct similar analysis using larger set of observations from drifters in 2015 and 2019 (approximately 11,000 and 1,200 data points respectively) that spanned different seasons to investigate mesoscale and sub-mesoscale variability. These observations are binned by $\delta(\Delta T_{diurnal})$ and drifter separation (Figure 4). During DWL-NC days, the $\delta(\Delta T_{diurnal})$ remain relatively uniform ($0.05\text{ }^{\circ}\text{C}$ median and $0.1\text{ }^{\circ}\text{C}$ 90th percentile values) across 0 to 100 km separation in both years (Figure 4). In contrast, DWL-C days exhibit higher $\delta(\Delta T_{diurnal})$ magnitudes. Median $\delta(\Delta T_{diurnal})$ are approximately $0.2\text{ }^{\circ}\text{C}$ and increase with separation (Figure 4). The 90th percentile values during DWL-C days also show greater variability. In 2019, differences of around $0.4\text{ }^{\circ}\text{C}$ over 20 km and about $0.8\text{ }^{\circ}\text{C}$ over 50–100 km are observed (Figure 4b). The differences of about $0.8\text{ }^{\circ}\text{C}$ over 20 km and up to $1.4\text{ }^{\circ}\text{C}$ over 100 km are observed in 2015 (Figure 4a). This points to enhanced spatial inhomogeneity in diurnal SSTs during DWL events.

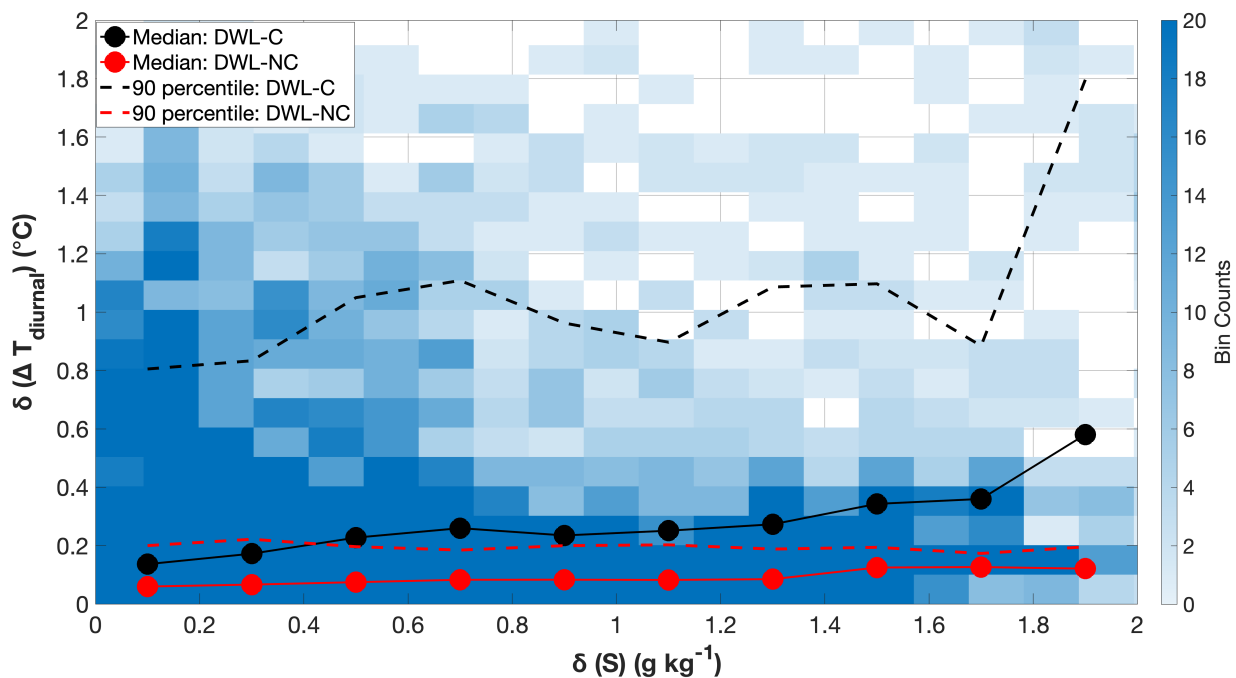


FIG. 5. Binned scatter plot of $\delta(\Delta T_{diurnal})$ in drifter pairs separated by less than 100 km against the in-situ surface salinity differences ($\delta(S)$, as a proxy for differences in vertical salinity stratification) for 01 September to 30 November 2015. Color indicates the number of observations per bin (every 0.1 g kg^{-1} and $0.1\text{ }^{\circ}\text{C}$). The solid line with circle markers indicate the median values in each bin of $\delta(S)$, segregated into DWL-C days (black) and DWL-NC days (red). The dashed lines indicate the 90th percentile values in each bin.

To test the hypothesis that lateral differences in salinity stratification influences diurnal SST variability, we use salinity differences ($\delta(S)$) between drifter pairs (with separation distances under 100 km) as a proxy for stratification differences and analyze their relationship with $\delta(\Delta T_{diurnal})$. We observe $\delta(S)$ up to 2 g kg^{-1} between drifter pairs, typical for the Bay of Bengal's Fall Intermonsoon given heavy rainfall and river runoff (e.g., Sree Lekha et al. 2018). Despite these large $\delta(S)$ values, the median and 90th percentile $\delta(\Delta T_{diurnal})$ values increase only by about 0.1–0.2 °C with increasing salinity stratification, regardless of DWL presence (Figure 5). This result aligns with anecdotal values from Shroyer et al. (2016), though it is lower than estimates from other studies (Soloviev and Lukas 1997; Moulin et al. 2021).

Our observations indicate that lateral differences in salinity stratification correlate with the $\delta(\Delta T_{diurnal})$ (black solid lines in Figure 4). However, the contribution of salinity stratification in $\delta(\Delta T_{diurnal})$ (Figure 5) falls short of accounting for the observed extreme values in $\delta(\Delta T_{diurnal})$ (black dotted lines in Figure 4). This suggests contributions in $\delta(\Delta T_{diurnal})$ from other factors (e.g., heat flux variability, wind, ocean optical properties, mixed layer depth), which are not measured by drifter observations.

However, these variables not measured by drifters may also introduce uncertainty in the binned relationships shown in Figure 5. In order to isolate the role of salinity stratification on $\Delta T_{diurnal}$ and $\delta(\Delta T_{diurnal})$, we next use the one-dimensional GOTM model to systematically assess its impact on $\delta(\Delta T_{diurnal})$.

5. Simulating the Influence of Salinity Stratification on $\Delta T_{diurnal}$ Variability

GOTM simulations are initialized with temperature and salinity profiles based on D-BASIS observations (Figure 6, discussed more in Section-6) to explore the influence of salinity stratification on $\Delta T_{diurnal}$. Salinity control of the upper ocean stratification is achieved through the initial MLD at sunrise and the initial salinity change at the base of the MLD (ΔS_b) illustrated in Figure 6b. GOTM simulations are forced with diurnally varying solar radiation peaking at 1000 W m^{-2} (based on Renner et al. 2019), with constant cooling components of heat fluxes and wind speeds over a 24-hour run. We explore the parameter space by varying the initial MLD (2–15 m), ΔS_b (0–1 g kg^{-1}), daily mean net heat flux (0, 33 and 123 W m^{-2} , achieved by adjusting the cooling components) and wind speeds ($3\text{--}6 \text{ ms}^{-1}$). We also vary the optical properties by using theoretical Jerlov-I

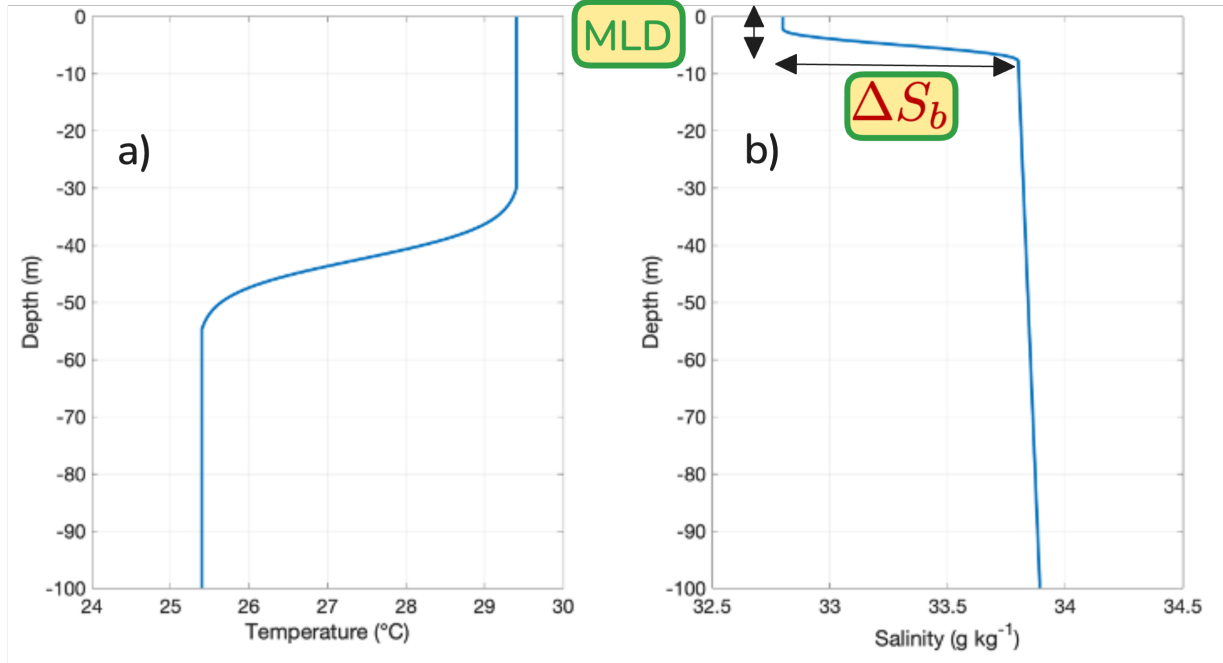


FIG. 6. Initial vertical profiles of a) Temperature and b) Salinity for GOTM parameter space exploration. The stratification in the initial profiles is controlled using the Mixed layer depth (MLD) and the change in salinity at the base of mixed layer (ΔS_b).

absorption profile (Paulson and Simpson 1977a) and an observed absorption profile derived from D-BASIS irradiance measurements (similar to equation-4 in Paulson and Simpson (1977b) with $R=0.4$, $\zeta_1 = 0.9 \text{ m}$, $\zeta_2 = 16.7 \text{ m}$, pers comm. Tamara Schlosser).

For a representative case (net heat flux of 123 W m^{-2} , Jerlov-I water type, 6 m s^{-1} winds) we observe little variation in $\Delta T_{diurnal}$ for deeper initial MLD and weaker ΔS_b (Figure 7a). However, the sensitivity of $\Delta T_{diurnal}$ to ΔS_b is relatively stronger for shallow MLDs between 2 and 4 m, with differences of $O(0.1 \text{ }^{\circ}\text{C})$. We fix the initial MLD to 4 m (where stratification-driven variability is strongest) to assess how changing net heat flux and wind speed affect $\Delta T_{diurnal}$ dependence on stratification. As expected, $\Delta T_{diurnal}$ varies with heat fluxes and wind speeds ($0.57\text{-}1.2 \text{ }^{\circ}\text{C}$). However, the $\delta(\Delta T_{diurnal})$ due to the salinity stratification variations (inferred from differences in $\Delta T_{diurnal}$ due to differences in ΔS_b) are within a range of $0.07\text{-}0.15 \text{ }^{\circ}\text{C}$ (Figure 7b). Varying optical properties has a relatively minor effect on the sensitivity of $\delta(\Delta T_{diurnal})$ due to the salinity stratification variations (Figure 7c).

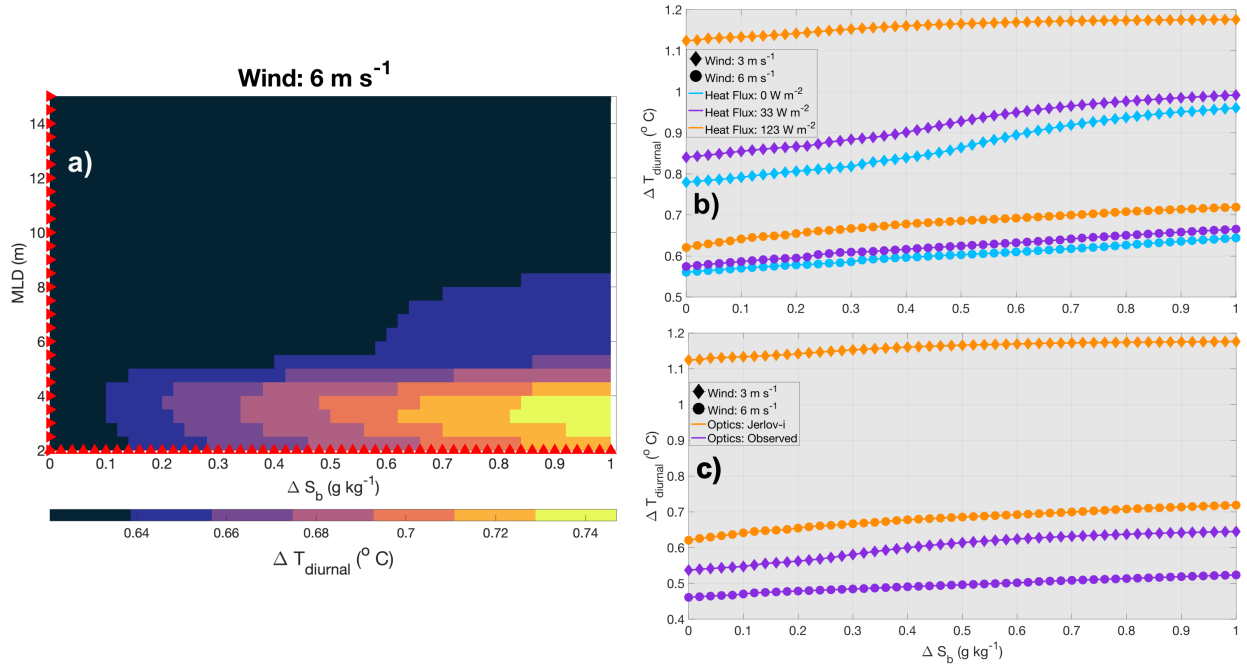


FIG. 7. a) $\Delta T_{diurnal}$ from GOTM as a function of change in salinity at the base of mixed layer (ΔS_b , in x-axis) and initial MLD (in y-axis) for a diurnally varying clear sky day with wind speed of 6 m s^{-1} and mean heat flux of 123 W m^{-2} . b) $\Delta T_{diurnal}$ as a function of initial change in salinity at the base of mixed layer of 4 m (ΔS_b) for different wind speeds (diamond and circle markers for 3 meter/s and 6 meter/s scenarios respectively) and daily mean heat fluxes. c) is same as b) but for varying wind speed and optical properties. The mean heat flux in this case is 123 W m^{-2} .

A comparison of our modeling results with the observed $\delta(\Delta T_{diurnal})$ from drifters indicates that the magnitude of median $\delta(\Delta T_{diurnal})$ during DWL days are consistent with those expected from lateral variations in salinity stratification, assuming minimal lateral variations in winds and heat fluxes over these scales (given that MLDs shallower than 10 m are a common feature in the Bay, e.g., Weller et al. 2019). However, the larger $\delta(\Delta T_{diurnal})$ in Figure 4 likely reflect combined effects of spatial variability in stratification, optical properties, wind speed, net heat flux, and cloud cover, all of which can vary on mesoscale and smaller length scales. The next section uses a D-BASIS example to illustrate how lateral stratification differences can shape subsurface DWL evolution.

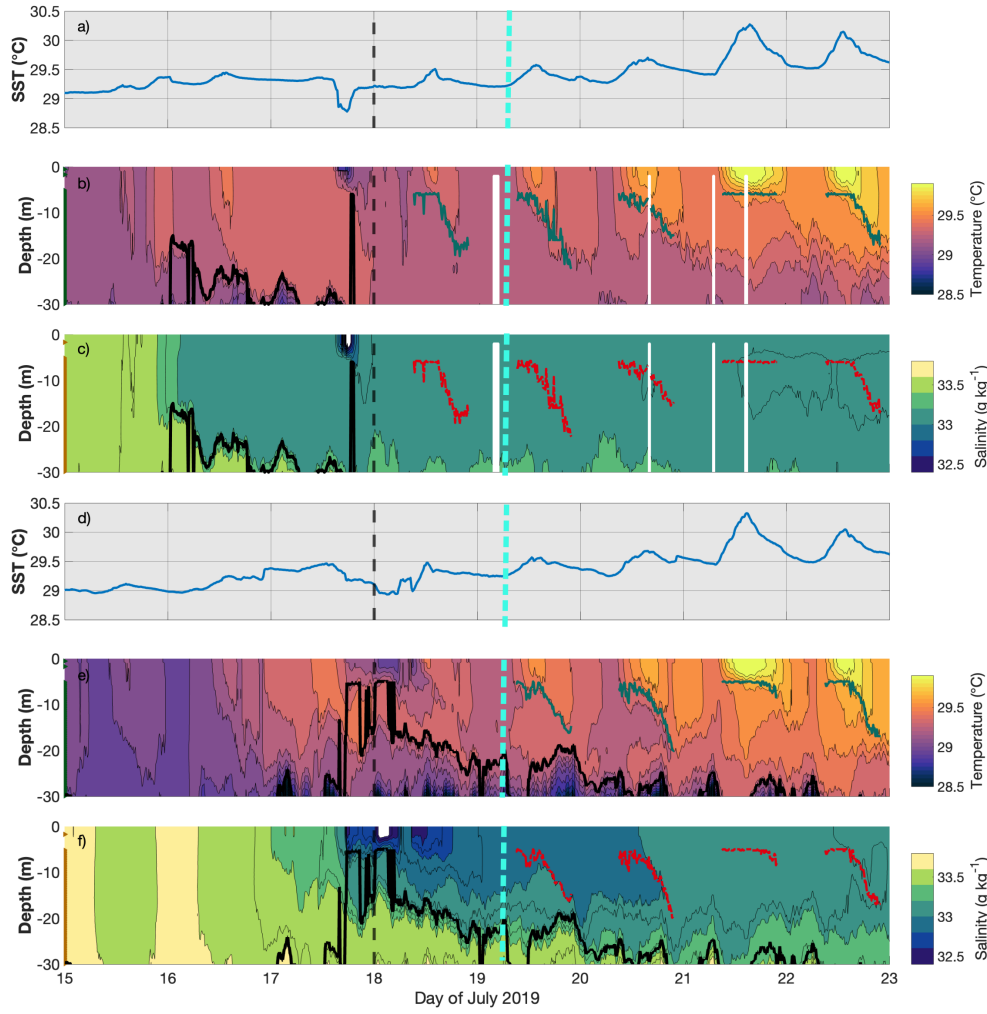


FIG. 8. a) Observed SST for D2, b) observed temperature and c) salinity at D2 from 15-22 July 2019. The measurements from the surface buoy are included in panel b) and c) as they were measured at 0.55 m and 1.7 meter depth. The green lines in panels b) as well as the red lines in panel c) indicate the DWL depth. The thick black lines in panels b) and c) indicate the seasonal pycnocline depth (where N^2 is greater than $5 \times 10^{-4} \text{ s}^{-2}$), while the contours in these panels represent isotherms and isohalines, separated by $0.1 \text{ }^\circ\text{C}$ and 0.1 g kg^{-1} , respectively. The markers at the left end of the panels b) and c) indicate the depths where the measurements were taken (continuous set of markers reflect the high resolution data density of the wirewalker below 5 m). The panels d), e), f) are similar to panels a), b), c) respectively for D3. The black dashed vertical lines in panels a-f indicate the beginning of the DWL period during the 2019 field campaign (see Appendix A), while the cyan dashed line marks the model initialization time in Figure 9. All time series are shown in local time (IST).

6. Impact of differences in Salinity-Driven Stratification on the Vertical Evolution of DWLs

The subsurface temperature profiles at D2 and D3 illustrate the DWL formation in the morning and their subsequent mixing by late afternoon during 18-22 July 2019 (Figure 8b,e). The DWL presence correlates with elevated daytime stratification (N^2) and shear (S), with N^2 up to two orders of magnitude and S up to one order of magnitude higher than on non-DWL days (Figure A4b,d,e).

Despite their proximity (20-40 km, Figure A1b) and similar surface forcing (wind speeds and heat fluxes), D2 and D3 exhibit differences in DWL evolution (Figure 8b,e). An example is the vertical evolution of DWLs on 19 July 2019, which differs due to variations in pre-existing salinity stratification between the two sites (Figure 8c,f). The average stratification over the top 15 m at sunrise (pre-DWL) is two orders of magnitude higher at D3 ($1.2 \times 10^{-4} \text{ s}^{-2}$) compared to D2 ($2.1 \times 10^{-6} \text{ s}^{-2}$, Figure 9a). Correspondingly, the MLD at sunrise (using the 0.125 kg m^{-3} density criterion) differs by about 20m between D3 and D2 (15m and 35m respectively). The contrast in pre-existing stratification and MLD before the DWL evolution at D2 and D3 (Figure 8) arises from a combination of mesoscale-structured stratification as well as the cold pool event (Appendix-B).

Despite notable differences in pre-existing stratification, D2 and D3 exhibit similar $\Delta T_{diurnal}$ of 0.34°C . This outcome is consistent with our parameter space exploration (Section 5), which indicates that the MLDs at D2 and D3 are beyond the range where stratification strongly influences $\Delta T_{diurnal}$. However, the stronger pre-existing stratification at D3 causes DWL depths to be shallower by about 8 m compared to D2 (Figure 9d). This suggests that pre-existing background stratification below the DWL primarily limits its vertical evolution through shear-driven mixing, thereby trapping the DWL to a shallower depth.

Idealized one-dimensional GOTM simulations, using initial profiles and surface forcing from D2 and D3, along with optical properties based on irradiance measurements from the D-BASIS (pers comm. Tamara Schlosser), successfully estimate the final DWL depth (Figure 9d). However, a detailed comparison of the time evolution of DWLs between the model and observations is not included. In the morning, the simulated DWLs are often shallower than the 5 m observational limit used to track DWL evolution based on temperature gradients. Although the DWL typically deepens in the afternoon, the observed evolution shows intermittent spikes that are likely caused by background oceanic processes, which are not represented in 1-D models.

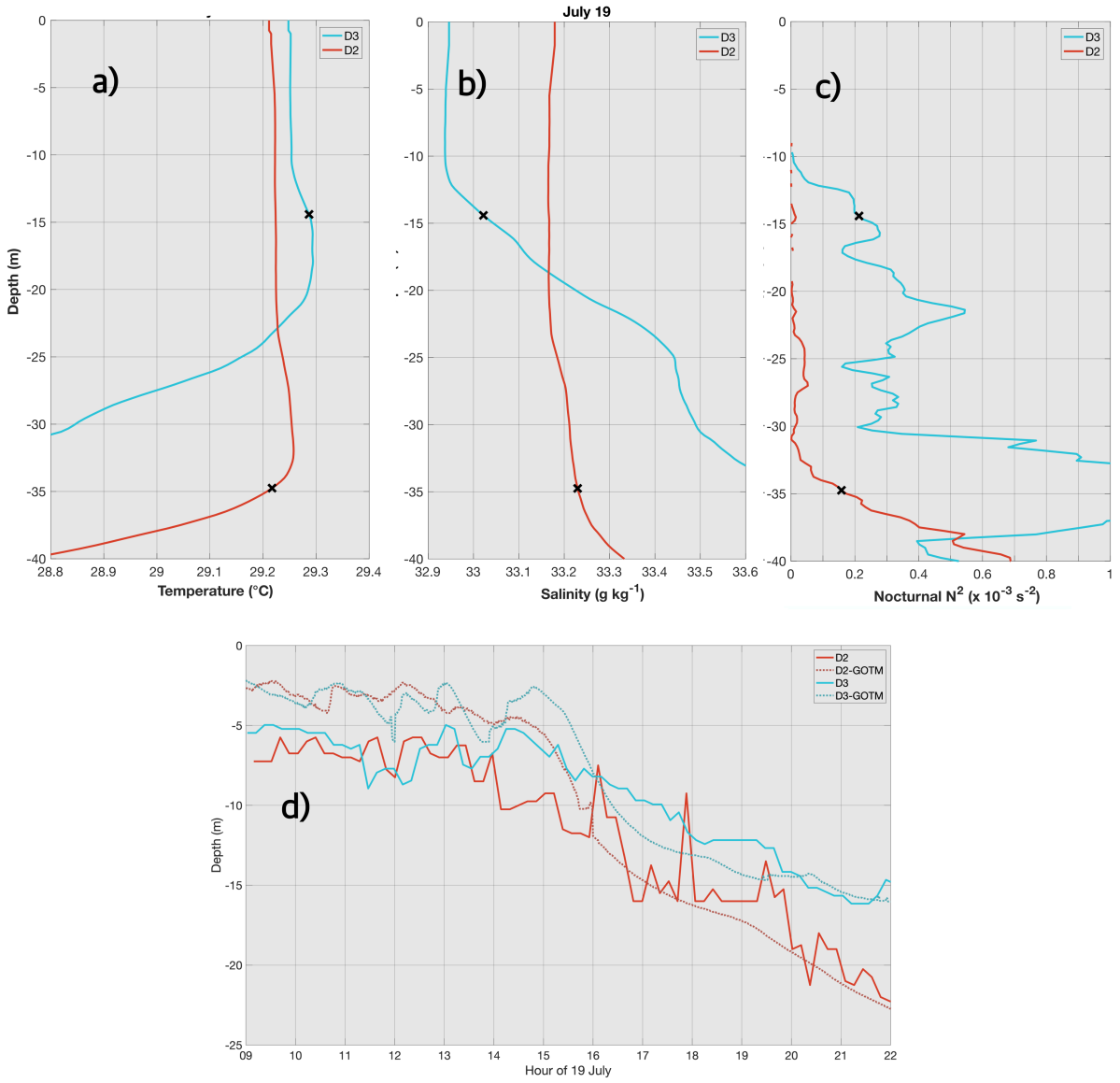


FIG. 9. a) Temperature, b) Salinity, c) Stratification profiles observed at D2 (red) and D3 (blue) just before sunrise on 19 July (cyan line in Figure 8). The two "x" marks indicate the respective MLDs based on the 0.125 kg m^{-3} criteria. d) Solid lines indicate the observed DWL depths at D2 and D3, while the dashed lines indicate the DWL depths from the corresponding GOTM simulations on 19 July 2019. Time series are shown in local time (IST).

Beyond pre-existing stratification differences, another example of varied DWL evolution between D2 and D3 stems from the advection of a rain lens (see Appendix-B of this paper; also Drushka et al. 2016). The DWL at D2 deepens steadily in a typical one-dimensional evolution to 20 m on

18 July 2019. The DWL at D3 in contrast remains confined above 5m due to stratification from the advected rain lens (see Appendix-B), and a subsurface warm layer develops (Figure 8d,e).

These observations collectively highlight how spatial variability in background stratification, rainfall and the advection of the resulting lens can lead to lateral differences in DWL evolution. Such differences cause lateral variability in upper ocean heat content and vertical mixing, consequently leading to lateral disparities in subsequent DWL evolution, air-sea feedback, and interfacial fluxes.

7. Discussion

The results presented here show ubiquitous lateral differences in diurnal SSTs ($\delta(\Delta T_{diurnal})$) of average magnitude 0.1-0.2 °C over scales as small as O(10 km). Our results also indicate that $\delta(\Delta T_{diurnal})$ are slightly larger on DWL conducive days than on non-conducive days. While solar insolation, wind speeds, and optical properties of water are known drivers of diurnal SST ($\Delta T_{diurnal}$) and $\delta(\Delta T_{diurnal})$ (e.g., Webster et al. 1996; Ohlmann 2003; Pimentel et al. 2019), our results show that variations in background salinity stratification (especially for regions like the Bay of Bengal) also play a role. This result is consistent with anecdotal examples in Shroyer et al. (2016). Although other studies report more drastic differences due to shallow freshwater lenses (e.g. Soloviev and Lukas 1997; Moulin et al. 2021), our idealized one-dimensional GOTM simulations produce $\delta(\Delta T_{diurnal})$ similar to those observed in the Bay of Bengal. These differences emerge only when the initial MLD (prior to DWL formation at sunrise) is shallow. However, such models may underestimate these values as Johnson et al. (2023) showed that one-dimensional turbulence closure models overestimate vertical entrainment at the base of the mixed layer on DWL days compared to Large Eddy Simulations (LES). To better constrain the role of salinity stratification in $\Delta T_{diurnal}$, longer-term co-located measurements of meteorological variables, $\Delta T_{diurnal}$, and ocean boundary layers, as well as analyses of high temporal and vertical resolution mooring records are needed.

D-BASIS observations from the 2019 field campaign reveal significant variations in background stratification over approximately 30 km. These variations play a role in driving lateral differences in sub-surface evolution of DWLs, which affect vertical heat distribution and can trigger submesoscale processes (Bogdanoff 2017). In addition to background stratification, lateral advection processes can cause lateral differences in DWLs (e.g. 18 July 2019 case). The advection could be caused

by lateral slumping of fronts due to submesoscale processes, differential advection or the profiler moving into a watermass of different stratification. Previous work has shown the existence of strong diurnal variations in the velocity shear near fronts (Dauhajre and McWilliams 2018; Johnson et al. 2020b) which further impact the stratification (Johnson et al. 2020a) and potentially influence the DWL evolution. Isolating these types of stratification changes using D-BASIS is difficult due to the inherent space-time aliasing.

DWLs are shown to be a regular feature in this region, with 188 occurrences recorded in 2015. Some of the DWL instances discussed here were also during the months of June to September (36 times in the year 2015), signaling their occurrence even when the monsoon season is prevalent in the Bay.

Modulation of air-sea fluxes and atmospheric convection by DWLs has traditionally been studied using a one-dimensional framework (e.g., Bellenger et al. 2010; de Szoek et al. 2021; Clayson and Bogdanoff 2013), with differences of $O(0.3\text{ }^{\circ}\text{C})$ in diurnal SSTs leading to $O(10\text{ W m}^{-2})$ differences in air-sea fluxes (Shevchenko et al. 2023). However, SST fronts influence atmospheric convection variability and create secondary circulations within the Marine Atmospheric Boundary layer (MABL, e.g., Sullivan et al. 2020, 2021; Skillingstad et al. 2007). Our observations of horizontal variability in DWLs further motivates the recent systematic modeling studies extending beyond laterally homogeneous coupled LES studies of Sullivan et al. (2025), incorporating multi-scale coupling between laterally variable DWLs and overlying MABL dynamics.

8. Conclusions

Remote sensing combined with in-situ observations reveals significant lateral differences in the diurnal SST amplitudes ($\delta(\Delta T_{diurnal})$) across a diverse range of sub-basin length scales in the Bay of Bengal. Using the day-night passes of the satellite AMSR-2, we observe $\delta(\Delta T_{diurnal})$ values of $O(1\text{ }^{\circ}\text{C})$ over mesoscale length scales of $O(100\text{ km})$ or larger. However, remote sensing poorly resolves the $\delta(\Delta T_{diurnal})$ when compared to a dense network of surface drifters and a mooring triad. The underestimation in $\delta(\Delta T_{diurnal})$ is especially pronounced in extreme cases where in-situ values reveal differences as high as $2\text{ }^{\circ}\text{C}$. Using the meteorological conditions from the mooring triad network to identify the conducive days for Diurnal Warm Layers (DWLs), we find that the $\delta(\Delta T_{diurnal})$ values are larger on DWL conducive days ($0.12\text{ }^{\circ}\text{C}$ median, $0.48\text{ }^{\circ}\text{C}$ 90th percentile)

when compared to the non-conducive DWL days (0.07°C median, 0.27°C 90th percentile). Data from a dense network of surface drifters deployed during the 2015 and 2019 field campaigns show similar trends over length scales of 1–100 km. On DWL days, median $\delta(\Delta T_{diurnal})$ values range from 0.05–0.2 °C, with 90th percentile values ranging from 0.2–1.4 °C. These ranges are smaller for non-DWL days, with the median differences ranging from 0.05–0.1 °C and 90th percentile values between 0.1–0.2 °C. Drifters equipped with surface salinity sensors further reveal that increasing lateral differences in surface salinity (a proxy for stratification differences) led to $\delta(\Delta T_{diurnal})$ of about 0.2 °C, regardless of DWL presence.

We use idealized one-dimensional modeling to explore how $\delta(\Delta T_{diurnal})$ varies with initial MLD and salinity stratification, under different wind speeds, optical properties, and heat fluxes. Our simulations confirm that the impact of salinity stratification on the $\delta(\Delta T_{diurnal})$ is about 0.07–0.15 °C, but only for very shallow MLDs (less than 8 m). This indicates that lateral variability in salinity-driven stratification (especially with shallow MLDs in the Bay) can modulate diurnal warming.

Our observations (using D-BASIS profilers) reveal lateral variability in the subsurface evolution of DWLs over scales of approximately 30 km. Lateral advection influences DWL structure, altering its penetration depth by 5–10 m. Additionally, pre-existing differences in stratification also impact this variability. These DWL differences affect the vertical distribution of heat within the upper ocean.

In summary, this study quantifies $\delta(\Delta T_{diurnal})$ over submesoscale and smaller mesoscale lengths, and highlights the role of differences in salinity stratification in driving these differences. Our results show that variations in salinity stratification alone cannot account for the extreme $\delta(\Delta T_{diurnal})$ values at these scales. These extreme $\delta(\Delta T_{diurnal})$ values could stem from small-scale coastal plumes causing optical property variations (McKie et al. 2024; Pimentel et al. 2019), or variations in wind speeds (Song et al. 2022) and heat fluxes (e.g., due to patchy clouds or differences in cooling components; Nuijens et al. 2024; Song et al. 2022). This study highlights the presence of small-scale lateral DWL variations that occur in regions with strong salinity gradients. Such salinity gradients are often unresolved in regional models (Vinayachandran and Nanjundiah 2009), potentially leading to an underestimation of diurnal SST and DWL gradients in these model simulations.

Acknowledgments. The authors would like to thank US Office of Naval Research for their support to the ASIRI as well as MISO-BoB Department Research Initiative. S.Kerhalkar and A.Tandon were supported by N00014-17-1-2355, N00014-18-1-2799, N00014-19-1-2410 and N00014-23-1-2054, J.T.Farrar by N00014-17-1-2880, J.A. MacKinnon by N00014-23-1-2056, T.L.Schlosser and A.J.Lucas by N00014-17-1-2391, L.Johnson by N00014-17-1-2393, V.Hormann and L.R.Centurioni by N00014-19-1-2691, N00014-13-1-0477, N00014-15-1-2286. A.Tandon was additionally supported by N00014-23-1-2473. The authors would also like to thank the Captain, crew and the science party of R/V Sally Ride during MISO-BoB Leg-2 for their help in data collection. S.K would like to thank the Associate Provost's office, University of Massachusetts Dartmouth for their support through the Distinguished Doctoral Fellowship. S.K is thankful to Emily Shroyer, Kenneth Hughes, Jonathan Nash, Eric D'Asaro, Christian Buckingham, Steven Lohrenz and Miles Sundermeyer for their stimulating discussions on various aspects of this work. The authors would like to express their sincere gratitude to the two anonymous reviewers and the editor, Dr. Gregory Foltz for their constructive suggestions, which greatly enhanced the quality and clarity of this manuscript.

Data availability statement. The NIOT mooring data are available at: <http://do.incois.gov.in/>. The WHOI mooring data from 2015 can be accessed at: <http://uop.whoi.edu/projects/Bengal/QCData.html>. The D-BASIS data and FastCTD data from 2019 as well as Surface Drifter data from 2015 and 2019 are available at: <http://bit.ly/4kP1f12>. [The link is for the review process only and a DOI for this dataset would be created once the MS is closer to publication]. AMSR-2 satellite data were obtained from www.remss.com, and rainfall estimates from IMERG were obtained from <https://gpm.nasa.gov/data/imerg>. The geostrophic currents are derived from AVISO (<https://www.aviso.altimetry.fr/>), a remotely sensed altimetry product. Simulations were performed using version 6.0 of the General Ocean Turbulence Model (GOTM), available at <https://gotm.net/portfolio/>.

APPENDIX A

Description of Conditions During the 2019 Field Campaign Using D-BASIS and Basis for DWL Thresholds

The D-BASIS profilers' ability to concurrently measure the air-sea fluxes and resolve OBL at a high vertical resolution is instrumental in understanding the conditions favorable for DWLs. Meteorological measurements from the D-BASIS profilers also allow us to classify the operational period of the 2019 field campaign (Figure A1a) into three distinct regimes. These regimes correspond to phases of the monsoon intra-seasonal variability (ISV) as the field campaign took place during the Southwest Monsoon Season in the Bay. These ISV's are characterized by active and break phases. Break phases feature clear skies, which leads to diurnal cycles in the SST and increased likelihood of DWLs. In contrast, the active phases feature steady high wind speeds, overcast conditions, high precipitation rates, leading to a suppression in the diurnal cycles of SST.

The period from 12–17 July 2019 was marked by moderate wind speeds ($6.2\text{--}8.7\text{ m s}^{-1}$, Figure A2a), persistent southwesterly winds associated with the Southwest Monsoon (Figure A2b), and clear skies with peak shortwave radiation nearing 1000 W m^{-2} (Figure A2e). Rainfall was absent except for a heavy rain event on 17 July (Appendix B, Figure A2d). Diurnal SST amplitudes of $0.1\text{--}0.2\text{ }^{\circ}\text{C}$ were observed, along with a $0.2\text{ }^{\circ}\text{C}$ increase in foundational SST (Figure A3a,b). These conditions suggest that the sampled region of the Bay was in a break phase of the ISV. However, the upper 30 m of the ocean remained relatively well mixed, and no signatures of DWL formation were observed (Figure A3c, A4b,d,e).

A drop of $4\text{ }^{\circ}\text{C}$ in air temperature is observed across the three D-BASIS profilers on 17 July (Figure A2c). This is also followed by very high precipitation rate of 80 mm h^{-1} (Figure A2d). These conditions indicate an atmospheric cold pool event (de Szoeke et al. 2017; Simoes-Sousa et al. 2022), which is followed by calm conditions with night-time cooling and diurnal warming on the next day. The net rainfall due to this cold pool event is about 75 mm and 101 mm at D2 and D3 respectively. Such events freshen the upper ocean and create rain lenses (Moulin et al. 2021; Iyer and Drushka 2021).

During the period of 18-22 July 2019, wind speeds ranged from $2.8\text{--}6.1\text{ m s}^{-1}$ (Figure A2a), predominantly from the west and northwest direction (which is uncharacteristic as the winds are typically south-westerly during the monsoons in the Bay, Figure A2b). Clear sky conditions with peak SWR of nearly 1000 W m^{-2} persisted during this period (Figure A2e). The diurnal SST amplitudes during this period are $0.5\text{--}0.8\text{ }^{\circ}\text{C}$ (or even more in some cases), with an increase of $0.25\text{ }^{\circ}\text{C}$ in the foundational SST (Figure A3a,b). These conditions indicate that the sampled part

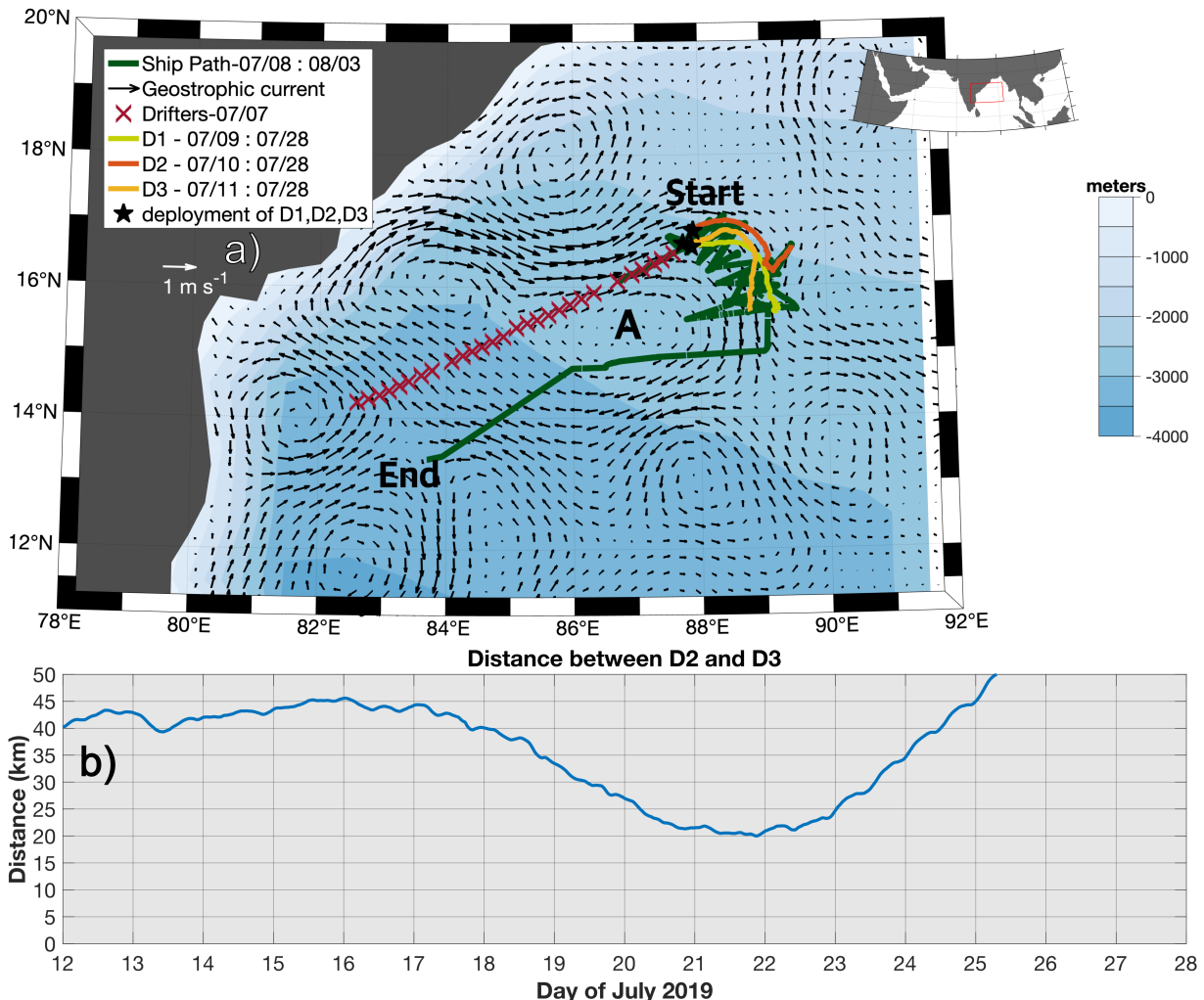


FIG. A1. a) Map of the Bay of Bengal displaying various assets used for sampling during the MISO-BoB Intensive Observational Period (IOP) in 2019. The legend provides information about the deployment dates and positions of drifters. It also includes deployment positions, paths, deployment dates, and recovery dates for the D-BASIS profilers (D1, D2, D3). The map also illustrates the ship's route and sampling dates. The background colors represent the bathymetry of the Bay, while the background arrows depict geostrophic currents averaged over a ten-day period from 15-24 July 2019. The letter A indicates the anticyclonic eddy along which the drifters moved. b) Time Series of separation distance between D2 and D3 profilers between 12 July to 27 July 2019. Time series is shown in local time (IST).

of the Bay was still in the break phase. However, the upper 30 m of the ocean exhibited strong stratification and shear along with enhanced temperature gradients, which are signatures consistent with the presence of DWLs. (Figure A3c, A4b,d,e, Hughes et al. 2020a).

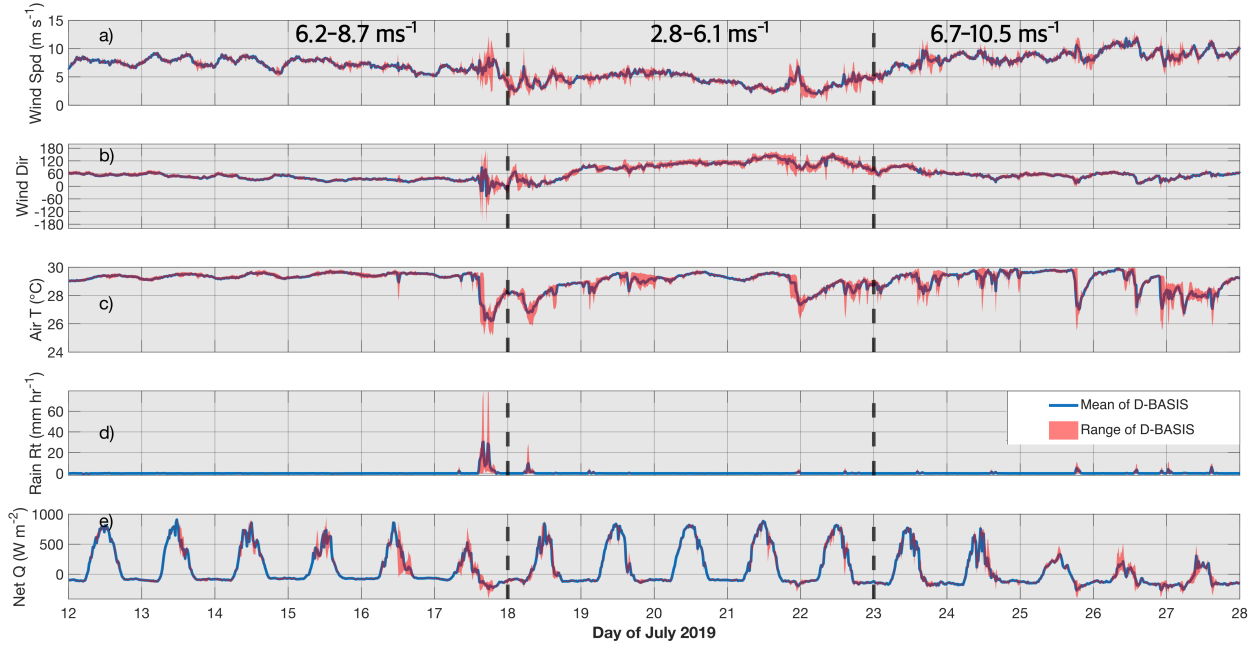


FIG. A2. Mean of Meteorological measurements from the three D-BASIS and averaged to 15-minute intervals in blue while the range between the three D-BASIS is indicated in red shaded area. a) Wind speeds, b) wind direction (0° indicates southerly winds whereas -90° angle indicates easterly winds), c) air temperature near the air-sea interface (2.65 m), d) precipitation rate and e) Net Heat Flux from 12 July to 27 July 2019. The 10th and 90th percentile values of wind speeds for each of the three periods from D-BASIS buoys are reported on panel a). The black dashed vertical lines in panels a–e are used to separate different periods described in Appendix A. All time series are shown in local time (IST).

During the remainder of the operational cruise period (23–28 July 2019), the wind speeds increased nearly two-fold from the previous period ($6.7\text{--}10.5\text{ ms}^{-1}$, Figure A2a) with the wind direction returning to the typical southwest monsoon pattern (Figure A2b). This period was also marked with steady rainfall at times (Figure A2d) and persistent overcast skies (with peak SWR of nearly 500 W m^{-2} , Figure A2e). As a result, the diurnal cycles in SST are suppressed and the foundational temperature gradually cools (Figure A3a,b). These conditions indicate that the sampled part of the Bay was in the active phase, with no possibility of DWLs due to lack of clear skies.

Based on the wind speeds observed during this field campaign, we define DWL-favorable conditions in the Bay as wind speeds below 6 ms^{-1} (at 3 m height). This limit is close to 7.6

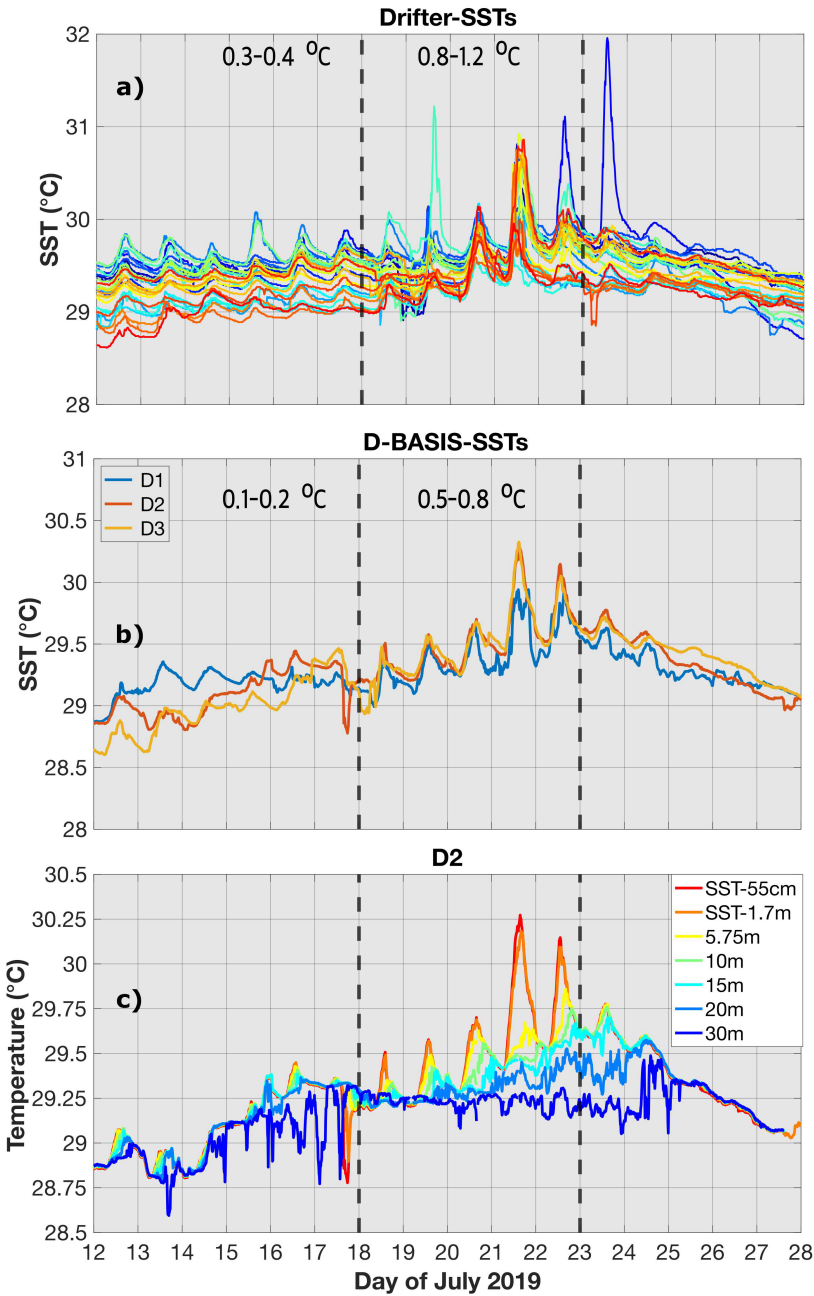


FIG. A3. Time series of SSTs as measured from a) drifters at 0.2 m depth, b) D-BASIS at 0.55 m and c) temperatures measured at various depths using D2 from 12 July to 27 July 2019. The typical diurnal cycles of SSTs for the periods where the diurnal cycles are prominent is reported on panels a) and b). The black dashed vertical lines in panels a–c are used to separate different periods described in Appendix A. All time series are shown in local time (IST).

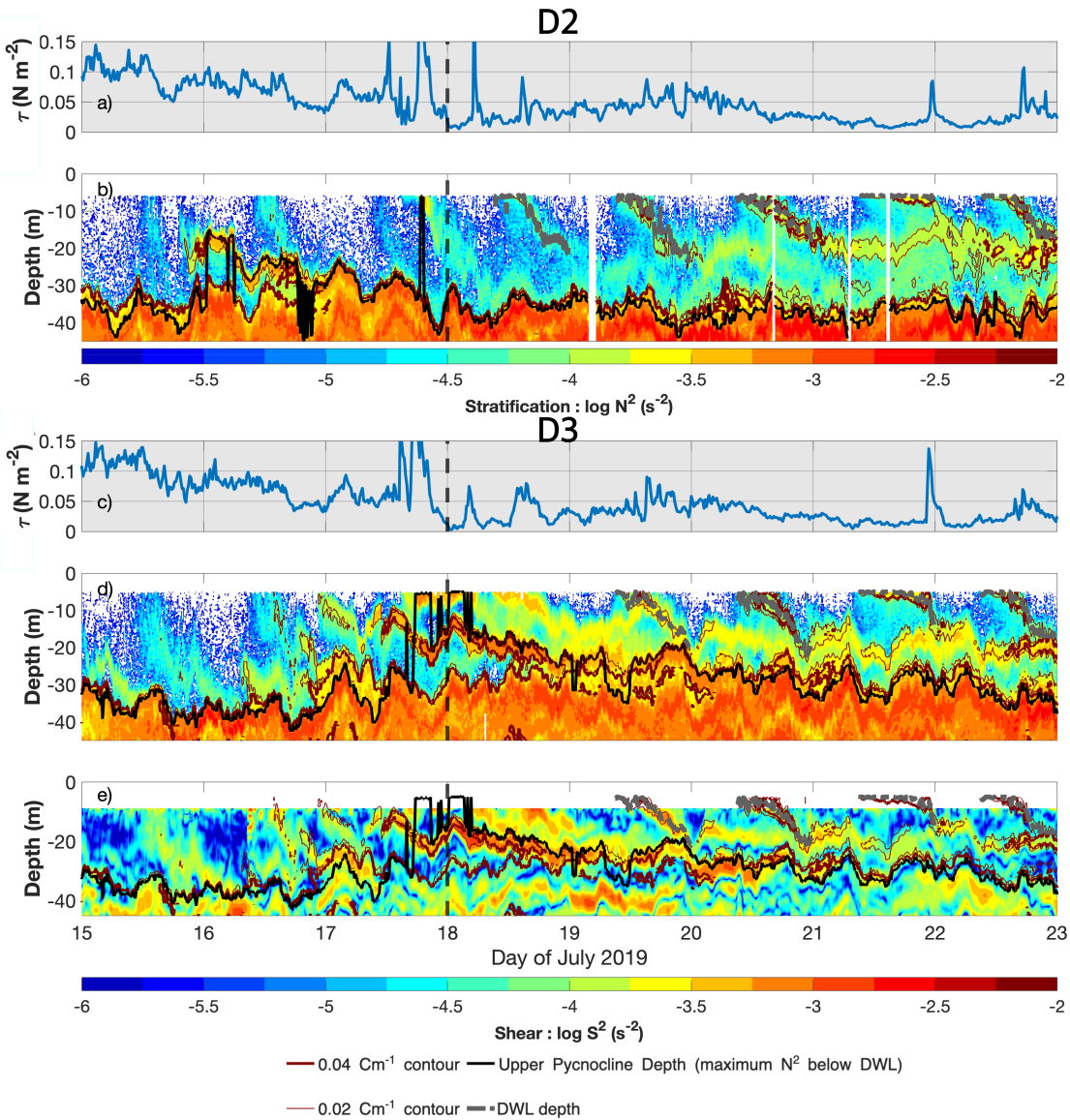


FIG. A4. a) Wind stress from D2. b) Stratification in logarithmic scale from D2 during 18 July to 22 July 2019. Panels c), d) are similar to panels a), b) respectively but for D3. e) Shear in logarithmic scale calculated from D3. Shear measurements from D2 are missing due to the loss of its ADCP. The thick brown contours in panels b), d), e) indicate the $0.04\ ^\circ C\ m^{-1}$ temperature gradient while the thin brown contour indicates the $0.02\ ^\circ C\ m^{-1}$ gradient. The gray dashed lines in panels b), d) and e) indicate the DWL depth. The thick black lines in panels b), c), e) indicate the upper pycnocline depth (based on the maximum N^2 below the typical DWL depth). The black dashed vertical lines in panels a–e indicate the beginning of the DWL period during the 2019 field campaign (see Appendix A). All time series are shown in local time (IST).

Transect	Date and Time Start	Date and Time End	Location Start	Location End
1	14 Jul 04:30	14 Jul 18:30	17.07 N, 88.4 E	16.35 N, 87.98 E
2	17 Jul 05:45	17 Jul 17:10	16.27 N, 88.2 E	16.88 N, 88.55 E
3	17 Jul 18:20	18 Jul 04:25	16.88 N, 88.55 E	16.27 N, 88.2 E
4	18 Jul 18:15	19 Jul 07:50	16.38 N, 89.13 E	16.05 N, 88.28 E
5	19 Jul 07:50	19 Jul 20:05	16.05 N, 88.28 E	16 N, 89.23 E

TABLE B1. Information about ship transects during the 2019 Field Campaign as shown in Figure B1. The times are reported as local time (UTC + 5.5 hours)

ms^{-1} (at 10 m height) defined for the wind speed limits for DWL formation in Equatorial Indian Ocean (Thompson et al. 2019). In addition, we use a peak SWR threshold of 750 W m^{-2} or greater to detect clear skies for DWL conditions (based on theoretical SWR calculations in Renner et al. 2019).

APPENDIX B

Evolution of Upper Ocean Structure Before and After the 17 July 2019 Coldpool Event

The cold pool event on 17 July 2019 triggered heavy rainfall, leading to the formation of freshwater lens. However, the variability in stratification in the sampling region is not solely controlled by this intense precipitation event. The FastCTD measurements from the ship showed significant gradients in stratification in the East-West direction even before the rainfall event (Transect-1, Figure B1a,b). Transect-2 cuts across the D3 path on 17 July 2019 such that the end of the ship transect (post-rainfall) overlaps with the start of D3 (pre-rainfall; Figure B1c). Similarity in the salinity structure between the two sources indicates that the shallow stratification existed before the cold pool event. Ship transects conducted on 19 July reveal greater spatial variability in upper ocean salinity structure compared to earlier transects, likely influenced by both the cold pool event and pre-existing mesoscale-structured stratification. (Figure B1e,f).

Focusing on the cold pool event, both ship and D-BASIS profilers (D2, D3) detected rain lens formation during Transect-3 (a repeat of Transect-2; Figure B1d, Figure 8c,f). The lens at D3 persisted longer than D2 due to stronger upper-ocean stratification at D3, consistent with observations from the tropical Pacific (Iyer and Drushka 2021). Between 17–18 July, near-surface salinity at D3 fluctuated even in the absence of recorded rainfall (Figure 8f, Figure A2d), likely due

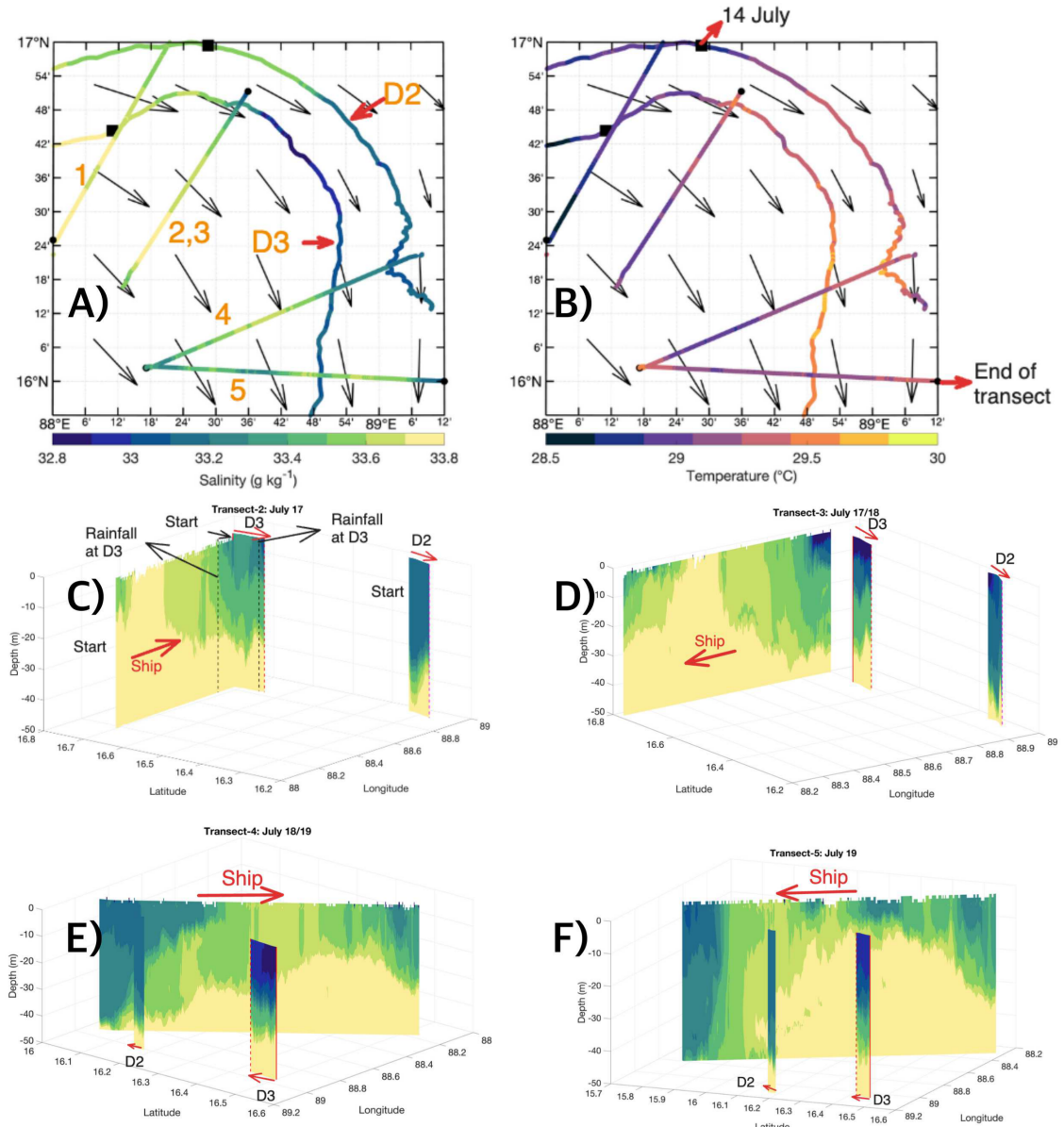


FIG. B1. a) Surface salinity and b) surface temperature observed from various ship transects, D2, and D3 during the 2019 field campaign. The start and end dates, along with the extents of each transect, are listed in Table B1. Black squares mark the positions of D2 and D3 on 14 July 2019, while black circles indicate the endpoints of each ship transect. c), d), e), and f) indicate 3-D plots of the salinity from ship transects 2, 3, 4, 5, as well as sections sampled from D2 and D3 during the same time, respectively (the color bar for these panels is the same as panel-a).

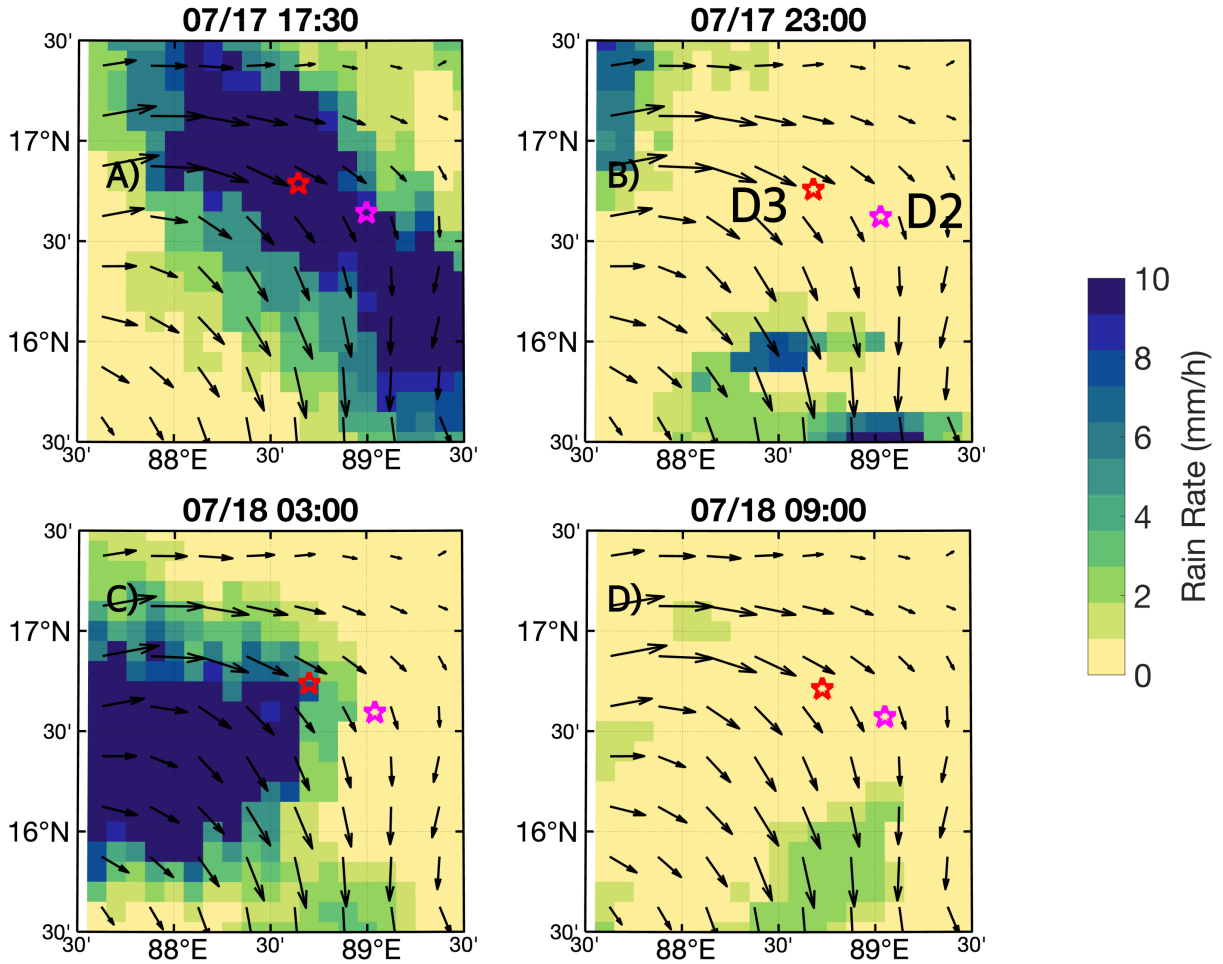


FIG. B2. Rainfall rates from IMERG at four different times (see subplot title for the time) on 17 and 18 July 2019 (Local Time). The magenta and red stars indicate the position of D2 and D3 respectively at the time of the snapshot from IMERG. The rainfall event in a) is captured at D2 and D3 (Figure A2d), while the rainfall around D3 in c) is not captured in the in-situ measurements.

to advection of nearby freshwater lens. IMERG imagery shows rainfall near D3 on 18 July at 03:00 (Figure B2c), not captured by in-situ rain gauges. Temperature fluctuations at D3 between 07:00 and 09:00 on 18 July (Figure 8e) further suggest D3 drifted through multiple lenses. These observations imply that lateral differences in background stratification may also result from advection of rain lens (similar to the movement of rain lenses as gravity current propagation in Moulin et al. 2021).

References

- Bellenger, H., and J.-P. Duvel, 2009: An analysis of tropical ocean diurnal warm layers. *Journal of Climate*, **22** (13), 3629–3646.
- Bellenger, H., Y. N. Takayabu, T. Ushiyama, and K. Yoneyama, 2010: Role of diurnal warm layers in the diurnal cycle of convection over the tropical Indian Ocean during MISMO. *Monthly Weather Review*, **138** (6), 2426–2433, <https://doi.org/10.1175/2010MWR3249.1>.
- Bogdanoff, A. S., 2017: Physics of diurnal warm layers: Turbulence, internal waves, and lateral mixing. Massachusetts Institute of Technology.
- Burchard, H., and K. Bolding, 2001: Comparative Analysis of Four Second-Moment Turbulence Closure Models for the Oceanic Mixed Layer. *Journal of Physical Oceanography*, **31** (8), 1943–1968, [https://doi.org/10.1175/1520-0485\(2001\)031<1943:CAOFSM>2.0.CO;2](https://doi.org/10.1175/1520-0485(2001)031<1943:CAOFSM>2.0.CO;2).
- Burchard, H., K. Bolding, T. P. Rippeth, A. Stips, J. H. Simpson, and J. Sündermann, 2002: Microstructure of turbulence in the Northern North Sea: A comparative study of observations and model simulations. *Journal of Sea Research*, **47** (3-4), 223–238.
- Burchard, H., K. Bolding, and M. R. Villarreal, 1999: *GOTM, a general ocean turbulence model: theory, implementation and test cases*. Space Applications Institute.
- Canuto, V. M., A. Howard, Y. Cheng, and M. Dubovikov, 2001: Ocean Turbulence. Part I: One-Point Closure Model—Momentum and Heat Vertical Diffusivities. *Journal of Physical Oceanography*, **31** (6), 1413–1426.
- Clayson, C. A., and A. S. Bogdanoff, 2013: The Effect of Diurnal Sea Surface Temperature Warming on Climatological Air–Sea Fluxes. *Journal of Climate*, **26** (8), 2546–2556.
- Dauhajre, D. P., and J. C. McWilliams, 2018: Diurnal Evolution of Submesoscale Front and Filament Circulations. *Journal of Physical Oceanography*, **48** (10), 2343–2361.
- de Szoëke, S. P., T. Marke, and W. A. Brewer, 2021: Diurnal ocean surface warming drives convective turbulence and clouds in the atmosphere. *Geophysical Research Letters*, **48** (4), e2020GL091299.

de Szoek, S. P., E. D. Skillingstad, P. Zuidema, and A. S. Chandra, 2017: Cold Pools and Their Influence on the Tropical Marine Boundary Layer. *Journal of the Atmospheric Sciences*, **74** (4), 1149–1168, <https://doi.org/10.1175/JAS-D-16-0264.1>.

Donlon, C., and Coauthors, 2007: The Global Ocean Data Assimilation Experiment High-resolution Sea Surface Temperature Pilot Project. *Bulletin of the American Meteorological Society*, **88** (8), 1197–1214.

Drushka, K., W. E. Asher, B. Ward, and K. Walesby, 2016: Understanding the formation and evolution of rain-formed fresh lenses at the ocean surface. *Journal of Geophysical Research: Oceans*, **121** (4), 2673–2689.

Entekhabi, D., and Coauthors, 2014: SMAP handbook—soil moisture active passive: Mapping soil moisture and freeze/thaw from space. *Jet Propulsion Lab., California Inst. Technol., Pasadena, Calif.*

Essink, S., V. Hormann, L. R. Centurioni, and A. Mahadevan, 2019: Can we detect submesoscale motions in drifter pair dispersion? *Journal of Physical Oceanography*, **49** (9), 2237–2254.

Fairall, C. W., E. F. Bradley, J. S. Godfrey, G. A. Wick, J. B. Edson, and G. S. Young, 1996b: Cool-skin and warm-layer effects on sea surface temperature. *Journal of Geophysical Research: Oceans*, **101** (C1), 1295–1308, <https://doi.org/10.1029/95JC03190>.

Fairall, C. W., E. F. Bradley, J. E. Hare, A. A. Grachev, and J. B. Edson, 2003: Bulk Parameterization of Air-Sea Fluxes: Updates and Verification for the COARE Algorithm. *Journal of Climate*, **16** (4), 571–591, [https://doi.org/10.1175/1520-0442\(2003\)016<0571:BPOASF>2.0.CO;2](https://doi.org/10.1175/1520-0442(2003)016<0571:BPOASF>2.0.CO;2).

Gentemann, C. L., P. J. Minnett, P. Le Borgne, and C. J. Merchant, 2008: Multi-satellite measurements of large diurnal warming events. *Geophysical Research Letters*, **35** (22).

Hormann, V., L. R. Centurioni, A. Mahadevan, S. Essink, E. A. D'Asaro, and B. P. Kumar, 2016: Variability of near-surface circulation and sea surface salinity observed from Lagrangian drifters in the northern Bay of Bengal during the waning 2015 southwest monsoon. *Oceanography*, **29** (2), 124–133.

- Huffman, G. J., D. T. Bolvin, D. Braithwaite, K. Hsu, R. Joyce, P. Xie, and S.-H. Yoo, 2015: NASA global precipitation measurement (GPM) integrated multi-satellite retrievals for GPM (IMERG). *Algorithm theoretical basis document (ATBD) version, 4 (26)*, 30.
- Hughes, K. G., J. N. Moum, and E. L. Shroyer, 2020a: Evolution of the Velocity Structure in the Diurnal Warm Layer. *Journal of Physical Oceanography*, **50** (3), 615–631, <https://doi.org/10.1175/JPO-D-19-0207.1>.
- Hughes, K. G., J. N. Moum, and E. L. Shroyer, 2020b: Heat Transport through Diurnal Warm Layers. *Journal of Physical Oceanography*, **50** (10), 2885–2905.
- Hughes, K. G., J. N. Moum, E. L. Shroyer, and W. D. Smyth, 2021: Stratified Shear Instabilities in Diurnal Warm Layers. *Journal of Physical Oceanography*.
- Imberger, J., 1985: The diurnal mixed layer. *Limnology and oceanography*, **30** (4), 737–770.
- Iyer, S., and K. Drushka, 2021: The Influence of Preexisting Stratification and Tropical Rain Modes on the Mixed Layer Salinity Response to Rainfall. *Journal of Geophysical Research: Oceans*, **126** (10), e2021JC017574.
- Johnson, L., B. Fox-Kemper, Q. Li, H. T. Pham, and S. Sarkar, 2023: A Finite-Time Ensemble Method for Mixed Layer Model Comparison. *Journal of Physical Oceanography*.
- Johnson, L., C. M. Lee, E. A. D'Asaro, L. Thomas, and A. Shcherbina, 2020a: Restratification at a California current upwelling front. Part I: Observations. *Journal of Physical Oceanography*, **50** (5), 1455–1472.
- Johnson, L., C. M. Lee, E. A. D'Asaro, J. O. Wenegrat, and L. N. Thomas, 2020b: Restratification at a California current upwelling front. Part II: Dynamics. *Journal of Physical Oceanography*, **50** (5), 1473–1487.
- Kondo, J., Y. Sasano, and T. Ishii, 1979: On Wind-Driven Current and Temperature Profiles with Diurnal Period in the Oceanic Planetary Boundary Layer. *Journal of Physical Oceanography*, **9** (2), 360–372.
- Lotliker, A. A., M. M. Omand, A. J. Lucas, S. R. Laney, A. Mahadevan, and M. Ravichandran, 2016: Penetrative Radiative Flux in the Bay of Bengal. *Oceanography*, **29** (2), 214–221.

MacKinnon, J. A., and Coauthors, 2021: A warm jet in a cold ocean. *Nature communications*, **12** (1), 2418.

Mahadevan, A., G. S. Jaeger, M. Freilich, M. M. Omand, E. L. Shroyer, and D. Sengupta, 2016: Freshwater in the Bay of Bengal. *Oceanography*, **29** (2), 72–81.

Marullo, S., P. J. Minnett, R. Santoleri, and M. Tonani, 2016: The diurnal cycle of sea-surface temperature and estimation of the heat budget of the Mediterranean Sea. *Journal of Geophysical Research: Oceans*, **121** (11), 8351–8367.

McKie, T., A. J. Lucas, and J. MacKinnon, 2024: Submesoscale dynamics in the Bay of Bengal: Inversions and instabilities. *Journal of Geophysical Research: Oceans*, **129** (3), e2023JC020563.

Merchant, C. J., M. J. Filipiak, P. Le Borgne, H. Roquet, E. Autret, J.-F. Piollé, and S. Laverder, 2008: Diurnal warm-layer events in the western Mediterranean and European shelf seas. *Geophysical Research Letters*, **35** (4), [https://doi.org/https://doi.org/10.1029/2007GL033071](https://doi.org/10.1029/2007GL033071).

Moulin, A. J., J. N. Moum, E. L. Shroyer, and M. Hoecker-Martínez, 2021: Freshwater lens fronts propagating as buoyant gravity currents in the equatorial Indian Ocean. *Journal of Geophysical Research: Oceans*, **126** (8), e2021JC017186.

Niiler, P. P., A. S. Sybrandy, K. Bi, P. M. Poulain, and D. Bitterman, 1995: Measurements of the water-following capability of holey-sock and TRISTAR drifters. *Deep Sea Research Part I: Oceanographic Research Papers*, **42** (11), 1951–1964, [https://doi.org/10.1016/0967-0637\(95\)00076-3](https://doi.org/10.1016/0967-0637(95)00076-3).

Nuijens, L., and Coauthors, 2024: The Air-Sea Interaction (ASI) submesoscale: physics and impact. *Lorentz Workshop*.

Ohlmann, J. C., 2003: Ocean radiant heating in climate models. *Journal of Climate*, **16** (9), 1337–1351.

Paulson, C. A., and J. J. Simpson, 1977a: Irradiance Measurements in the Upper Ocean. *Journal of Physical Oceanography*, **7** (6), 952–956, [https://doi.org/10.1175/1520-0485\(1977\)007<0952:IMITUO>2.0.CO;2](https://doi.org/10.1175/1520-0485(1977)007<0952:IMITUO>2.0.CO;2).

Paulson, C. A., and J. J. Simpson, 1977b: Irradiance measurements in the upper ocean. *Journal of Physical Oceanography*, **7** (6), 952–956.

Pimentel, S., K. Haines, and N. Nichols, 2008: Modeling the diurnal variability of sea surface temperatures. *Journal of Geophysical Research: Oceans*, **113** (C11).

Pimentel, S., W.-H. Tse, H. Xu, D. Denaxa, E. Jansen, G. Korres, I. Mirouze, and A. Storto, 2019: Modeling the near-surface diurnal cycle of sea surface temperature in the Mediterranean Sea. *Journal of Geophysical Research: Oceans*, **124** (1), 171–183.

Pinkel, R., M. A. Goldin, J. A. Smith, O. M. Sun, A. A. Aja, M. N. Bui, and T. Hughen, 2011: The Wirewalker: A Vertically Profiling Instrument Carrier Powered by Ocean Waves. *Journal of Atmospheric and Oceanic Technology*, **28** (3), 426–435, <https://doi.org/10.1175/2010JTECHO805.1>.

Pradhan, M., S. A. Rao, A. Bhattacharya, and S. Balasubramanian, 2022: Improvements in Diurnal Cycle and its Impact on Seasonal Mean by Incorporating COARE flux Algorithm in CFS. *Frontiers in Climate*, 198.

Price, J. F., R. A. Weller, and R. Pinkel, 1986: Diurnal cycling: Observations and models of the upper ocean response to diurnal heating, cooling, and wind mixing. *Journal of Geophysical Research: Oceans*, **91** (C7), 8411–8427, <https://doi.org/10.1029/JC091iC07p08411>.

Prytherch, J., J. T. Farrar, and R. A. Weller, 2013: Moored surface buoy observations of the diurnal warm layer. *Journal of Geophysical Research: Oceans*, **118** (9), 4553–4569, <https://doi.org/10.1002/jgrc.20360>.

Rao, R. R., and R. Sivakumar, 2003: Seasonal variability of sea surface salinity and salt budget of the mixed layer of the north Indian Ocean. *Journal of Geophysical Research: Oceans*, **108** (C1), 9–14, <https://doi.org/10.1029/2001JC000907>.

Renner, M., M. Wild, M. Schwarz, and A. Kleidon, 2019: Estimating shortwave clear-sky fluxes from hourly global radiation records by quantile regression. *Earth and Space Science*, **6** (8), 1532–1546.

Schmitt, M., H. Pham, S. Sarkar, K. Klingbeil, and L. Umlauf, 2024: Diurnal warm layers in the ocean: Energetics, nondimensional scaling, and parameterization. *Journal of Physical Oceanography*, **54** (4), 1037–1055.

Sengupta, D., G. N. Bharath Raj, M. Ravichandran, J. Sree Lekha, and F. Papa, 2016: Near-surface salinity and stratification in the north Bay of Bengal from moored observations. *Geophysical Research Letters*, **43** (9), 4448–4456, <https://doi.org/10.1002/2016GL068339>.

Sengupta, D., G. N. Bharath Raj, and S. S. C. Shenoi, 2006: Surface freshwater from Bay of Bengal runoff and Indonesian Throughflow in the tropical Indian Ocean. *Geophysical Research Letters*, **33** (22), <https://doi.org/10.1029/2006GL027573>.

Sengupta, D., and M. Ravichandran, 2001: Oscillations of Bay of Bengal sea surface temperature during the 1998 Summer Monsoon. *Geophysical Research Letters*, **28** (10), 2033–2036, <https://doi.org/10.1029/2000GL012548>.

Seo, H., A. C. Subramanian, A. J. Miller, and N. R. Cavanaugh, 2014: Coupled impacts of the diurnal cycle of sea surface temperature on the Madden–Julian oscillation. *Journal of Climate*, **27** (22), 8422–8443.

Shcherbina, A. Y., E. A. D’Asaro, and R. R. Harcourt, 2019: Rain and Sun Create Slippery Layers in Eastern Pacific Fresh Pool. *Oceanography (Washington, DC)*, **32** (2), 98.

Shenoi, S. S. C., D. Shankar, and S. R. Shetye, 2002: Differences in heat budgets of the near-surface Arabian Sea and Bay of Bengal: Implications for the summer monsoon. *Journal of Geophysical Research: Oceans*, **107** (C6), 5–14, <https://doi.org/10.1029/2000JC000679>.

Shevchenko, R., C. Hohenegger, and M. Schmitt, 2023: Impact of diurnal warm layers on atmospheric convection. *Journal of Geophysical Research: Atmospheres*, **128** (14), e2022JD038473.

Shroyer, E. L., D. L. Rudnick, J. T. Farrar, B. Lim, S. K. Venayagamoorthy, L. C. St. Laurent, A. Garanaik, and J. N. Moum, 2016: Modification of Upper-Ocean Temperature Structure by Subsurface Mixing in the Presence of Strong Salinity Stratification. *Oceanography*, **29** (2), 62–71.

Shroyer, E. L., and Coauthors, 2021: Bay of Bengal Intraseasonal Oscillations and the 2018 Monsoon Onset. *Bulletin of the American Meteorological Society*, 1–44, <https://doi.org/10.1175/bams-d-20-0113.1>.

Simoes-Sousa, I. T., A. Tandon, J. Buckley, D. Sengupta, E. Shroyer, and S. P. de Szoeke, 2022: Atmospheric Cold Pools in the Bay of Bengal. *Journal of the Atmospheric Sciences*.

Skyllingstad, E. D., D. Vickers, L. Mahrt, and R. Samelson, 2007: Effects of mesoscale sea-surface temperature fronts on the marine atmospheric boundary layer. *Boundary-layer meteorology*, **123**, 219–237.

Soloviev, A., and R. Lukas, 1997: Observation of large diurnal warming events in the near-surface layer of the western equatorial Pacific warm pool. *Deep Sea Research Part I: Oceanographic Research Papers*, **44 (6)**, 1055–1076, [https://doi.org/10.1016/S0967-0637\(96\)00124-0](https://doi.org/10.1016/S0967-0637(96)00124-0).

Soloviev, A., and R. Lukas, 2006: NEAR-SURFACE TURBULENCE BT - The Near-Surface Layer of the Ocean: Structure, Dynamics and Applications. Springer Netherlands, Dordrecht, 143–217, https://doi.org/10.1007/1-4020-4053-9_3, URL https://doi.org/10.1007/1-4020-4053-9_3.

Song, X., X. Xie, B. Qiu, H. Cao, S.-P. Xie, Z. Chen, and W. Yu, 2022: Air-sea latent heat flux anomalies induced by oceanic submesoscale processes: an observational case study. *Frontiers in Marine Science*, **9**, 850 207.

Song, Y., X. Yang, Y. Bao, F. Qiao, and Z. Song, 2024: Role of strong sea surface temperature diurnal variation in triggering the summer monsoon onset over the Bay of Bengal in a climate model. *Geophysical Research Letters*, **51 (15)**, e2023GL108 015.

Sree Lekha, J., J. M. Buckley, A. Tandon, and D. Sengupta, 2018: Subseasonal dispersal of freshwater in the northern Bay of Bengal in the 2013 summer monsoon season. *Journal of Geophysical Research: Oceans*, **123 (9)**, 6330–6348.

Sree Lekha, J., A. J. Lucas, J. Sukhatme, J. K. Joseph, M. Ravichandran, N. Suresh Kumar, J. T. Farrar, and D. Sengupta, 2020: Quasi-Biweekly Mode of the Asian Summer Monsoon Revealed in Bay of Bengal Surface Observations. *Journal of Geophysical Research: Oceans*, **125 (12)**, e2020JC016 271.

- Stuart-Menteth, A., I. Robinson, R. Weller, and C. Donlon, 2005: Sensitivity of the diurnal warm layer to meteorological fluctuations part 1: observations. *Journal of Atmospheric and Ocean Science*, **10** (3), 193–208.
- Sullivan, P. P., J. C. McWilliams, and E. G. Patton, 2025: An Investigation of Coupled Atmospheric and Oceanic Boundary Layers Using Large-Eddy Simulation. *Journal of the Atmospheric Sciences*, **82** (4), 829–846.
- Sullivan, P. P., J. C. McWilliams, J. C. Weil, E. G. Patton, and H. J. Fernando, 2020: Marine boundary layers above heterogeneous SST: Across-front winds. *Journal of the Atmospheric Sciences*, **77** (12), 4251–4275.
- Sullivan, P. P., J. C. McWilliams, J. C. Weil, E. G. Patton, and H. J. Fernando, 2021: Marine boundary layers above heterogeneous SST: Alongfront winds. *Journal of the Atmospheric Sciences*, **78** (10), 3297–3315.
- Sutherland, G., L. Marié, G. Reverdin, K. H. Christensen, G. Broström, and B. Ward, 2016: Enhanced Turbulence Associated with the Diurnal Jet in the Ocean Surface Boundary Layer. *Journal of Physical Oceanography*, **46** (10), 3051–3067, <https://doi.org/10.1175/JPO-D-15-0172.1>.
- Thompson, E. J., J. N. Moum, C. W. Fairall, and S. A. Rutledge, 2019: Wind limits on rain layers and diurnal warm layers. *Journal of Geophysical Research: Oceans*, **124** (2), 897–924.
- Vinayachandran, P., and R. S. Nanjundiah, 2009: Indian ocean sea surface salinity variations in a coupled model. *Climate dynamics*, **33**, 245–263.
- Webster, P. J., C. A. Clayson, and J. A. Curry, 1996: Clouds, radiation, and the diurnal cycle of sea surface temperature in the tropical western Pacific. *Journal of Climate*, **9** (8), 1712–1730.
- Weller, R., J. Farrar, H. Seo, C. Prend, D. Sengupta, J. S. Lekha, M. Ravichandran, and R. Venkatesen, 2019: Moored observations of the surface meteorology and air-sea fluxes in the northern Bay of Bengal in 2015. *Journal of Climate*, **32** (2), 549–573.
- Weller, R. A., and Coauthors, 2016: Air-Sea Interaction in the Bay of Bengal. *Oceanography*, **29** (2), 28–37.

Wentz, F. J., T. Meissner, C. Gentemann, K. A. Hilburn, and J. Scott, 2014: Remote Sensing Systems GCOM-W1 AMSR2 Daily Environmental Suite on 0.25 deg grid, Version 8.2,. Santa Rosa, CA, Remote Sensing Systems.

Wijesekera, H. W., and Coauthors, 2016: ASIRI: An Ocean–Atmosphere Initiative for Bay of Bengal. *Bulletin of the American Meteorological Society*, **97** (10), 1859–1884, <https://doi.org/10.1175/BAMS-D-14-00197.1>.

Zheng, B., A. J. Lucas, R. Pinkel, and A. Le Boyer, 2022: Fine-Scale Velocity Measurement on the Wirewalker Wave-Powered Profiler. *Journal of Atmospheric and Oceanic Technology*, **39** (2), 133–147.